Inorganic Chemistry

Article

pubs.acs.org/IC

Anticancer Activity and DNA Binding of a Bifunctional Ru(II) Arene Aqua-Complex with the 2,4-Diamino-6-(2-pyridyl)-1,3,5-triazine Ligand

Natalia Busto,[†] Jesús Valladolid,[†] Marta Martínez-Alonso,[†] Héctor J. Lozano,[†] Félix A. Jalón,[‡] Blanca R. Manzano,[‡] A. M. Rodríguez,[⊥] M. Carmen Carrión,[‡,§] Tarita Biver,[∥] José M. Leal,[†] Gustavo Espino,*[,†] and Begoña García*[,†]

[†]Departamento de Química, Facultad de Ciencias, Universidad de Burgos, Plaza Misael Bañuelos s.n., 09001, Burgos, Spain

[‡]Departamento de Química Inorgánica, Orgánica y Bioquímica, Facultad de Ciencias y Tecnologías Químicas-IRICA, Universidad de Castilla-La Mancha, Avda. Camilo José Cela, 10, 13071, Ciudad Real, Spain

[§]Fundación PCYTA, Paseo de la Innovación, 1, Edificio Emprendedores, 02006 Albacete, Spain

[∥]Dipartimento di Chimica e Chimica Industriale, Università di Pisa, 56126, Pisa, Italy

[⊥]Departamento de Química Inorgánica, Orgánica y Bioquímica, Escuela Técnica Superior de Ingenieros, Universidad de Castilla-La Mancha, Avda. Camilo José Cela, 10, 13071, Ciudad Real, Spain

Supporting Information

ABSTRACT: The synthesis and full characterization of the new aqua-complex $[(\eta^6\text{-}p\text{-cymene})Ru(OH_2)(\kappa^2\text{-}N,N\text{-2-pydaT})](BF_4)_2$, $[\mathbf{2}](\mathbf{BF_4})_2$, and the nucleobase derivative $[(\eta^6\text{-}p\text{-cymene})Ru(9\text{-MeG})(\kappa^2\text{-}N,N\text{-2-pydaT})](BF_4)_2$, $[\mathbf{4}](\mathbf{PF_6})_2$, where 2-pydaT = 2,4-diamino-6-(2-pyridyl)-1,3,5-triazine and 9-MeG = 9-methylguanine, are reported here. The crystal structures of both $[\mathbf{4}](\mathbf{PF_6})_2$ and the chloro complex $[(\eta^6\text{-}p\text{-cymene})RuCl(\kappa^2\text{-}N,N\text{-2-pydaT})](PF_6)$, $[\mathbf{1}](\mathbf{PF_6})$, have been elucidated by X-ray diffraction. The former provided relevant information regarding the interaction of the metallic fragment $[(\eta^6\text{-}p\text{-cymene})Ru(\kappa^2\text{-}N,N\text{-2-pydaT})]^{2+}$ and a simple model of DNA. NMR and kinetic absorbance studies have proven that the aqua-complex $[\mathbf{2}](\mathbf{BF_4})_2$ binds to the N7 site of guanine in nucleobases, nucleotides, or DNA. A stable bifunctional interaction (covalent and partially intercalated) between the $[(\eta^6\text{-}p\text{-cymene})Ru(\kappa^2\text{-}N,N\text{-2-pydaT})]^{2+}$ fragment and CT-DNA has been corroborated by kinetic, circular dichroism, viscometry, and thermal denaturation experiments. The reaction mechanism entails the very fast formation of the Ru−O-(PO_3) linkage prior to the fast intercalation of the 2-pydaT fragment. Then, a Ru−N7-(G) covalent bond is formed at the expense of the Ru−O-(PO_3) bond, yielding a bifunctional complex. The dissociation rate of the intercalated fragment is slow, and this confers additional interest to $[\mathbf{2}](\mathbf{BF_4})_2$ in view of the likely correlation between slow dissociation and biological activity, on the assumption that DNA is the only biotarget. Furthermore, $[\mathbf{2}](\mathbf{BF_4})_2$ displays notable pH-dependent cytotoxic activity in human ovarian carcinoma cells (A2780, IC_{50} = 11.0 μM at pH = 7.4; IC_{50} = 6.58 μM at pH = 6.5). What is more, complex $[\mathbf{2}](\mathbf{BF_4})_2$ is not cross-resistant with cisplatin, exhibiting a resistance factor, RF(A2780cis), of 0.28, and it shows moderate selectivity toward the cancer cell lines, in particular, A2780cis (IC_{50} = 3.0 5 ± 0.08 μM), relative to human lung fibroblast cells (MRC-5; IC_{50} = 24 μM), the model for healthy cells.

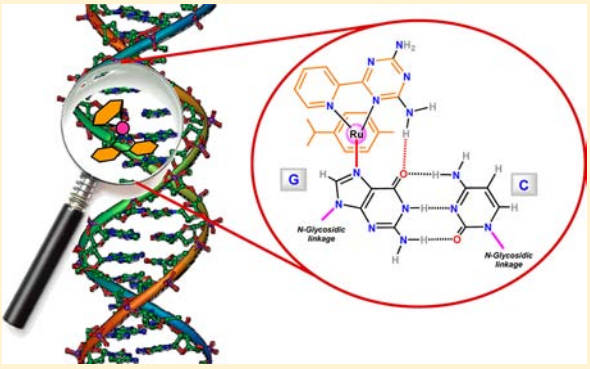

INTRODUCTION

Since the serendipitous discovery of the therapeutic activity of cisplatin and its derivatives against cancer, there has been a great deal of interest in developing new metallodrugs.[1] Cisplatin and its analogues carboplatin and oxaliplatin have been successfully used against several cancers (testicular, ovarian, cervical, head, neck, and lung cancers); however, their clinical use somehow is counteracted by their toxicity and the acquired resistance of some tumor cells to cisplatin.[2,3] Even though the biological activity of cisplatin has been ascribed to different signaling pathways, in fact it is primarily related to its interaction with chromosomal DNA by means of inter- or intrastrand cross-linking and DNA−protein cross-linking as well.[3,4]

Nowadays, an active research area is focused on the development of new metallodrugs capable of interacting with DNA, and organometallic ruthenium complexes are promising candidates to this aim.[5−11] Over the past few years, a huge amount of work has been published on the synthesis,

Received: May 15, 2013
Published: August 20, 2013

cytotoxicity, and DNA binding ability of this type of compounds; in particular, clinical trials have been done on NAMI-A and KP1019,[12] whose action is based on the activation by reduction of Ru(III) to Ru(II). Moreover, synthesized Ru(II) arene complexes such as RM175[13] or RAPTA-T[14] have shown both in vitro and in vivo anticancer activity.

Recently, we have reported on the cytotoxic activity of new Ru(II) arene complexes with aminophosphines[15] and on the biological activity and DNA binding properties of a new Ru(II) arene complex bearing a diamino−triazine ligand, [(η^6-*p*-cymene)RuCl(κ^2-*N*,*N*-2-pydaT)]BF_4, [**1**]($\mathbf{BF_4}$),[16] (Scheme 1),

Scheme 1. Structure and Numbering of the Ru^{II}-Arene Compounds [1](BF_4), [1](PF_6), [2](BF_4)$_2$, and [3](BF_4)

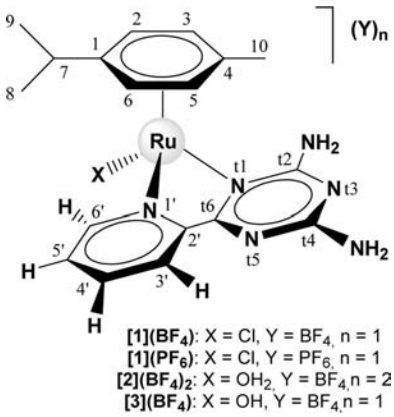

a complex species capable of interacting with DNA both externally and by groove binding. However, cytotoxicity and genotoxicity effects have not been observed in the studied cell lines.[16] These results and others reported with different types of metal complexes with Cl^- as the leaving group[17−19] reveal that the corresponding aqua-derivatives are more reactive to DNA. However, the corresponding aqua-complex partners have rarely been isolated and studied so far.

In this work, we have isolated the aqua-complex [(η^6-*p*-cymene)Ru(OH_2)(κ^2-*N*,*N*-2-pydaT)](BF_4)$_2$, [**2**]($\mathbf{BF_4}$)$_2$, and have also studied its interaction with DNA and its cytotoxic activity, including selectivity tests. Interestingly, [**2**]($\mathbf{BF_4}$)$_2$ interacts with DNA by a combination of binding modes that differ from those reported for the system [**1**]($\mathbf{BF_4}$)/DNA. Indeed, whereas the latter binds with DNA only externally,[16] [**2**]($\mathbf{BF_4}$)$_2$ gives way to a bifunctional covalent-intercalated complex, which is formed by a three-step mechanism. First of all, two fast processes are observed, namely, coordination of the metal ion to the phosphate group and intercalation. Presumably, the diamino-triazine ligand plays a fundamental role in the intercalation process. In the second place, a slow process attributed to covalent binding between the Ru(II) metal center and the N7 guanine site is unveiled by ^{1}H NMR and absorbance kinetic measurements. To the best of our knowledge, such a bifunctional behavior, fully characterized by a kinetic approach, has not been reported hitherto.

All these features, along with the cytotoxic activity observed in several cell lines, the satisfactory activity towards the cisplatin-resistant cell line, and the moderate selectivity versus healthy cells bear out the aqua-complex as a very interesting metallo-drug species.

RESULTS AND DISCUSSION

Preparation and Characterization of [2](BF_4)$_2$. We have recently reported on the synthesis of [(η^6-*p*-cymene)RuCl(κ^2-*N*,*N*-2-pydaT)](BF_4), [**1**]($\mathbf{BF_4}$), and provided spectroscopic evidence for the formation of the aqua-derivative [(η^6-*p*-cymene)Ru(OH_2)(κ^2-*N*,*N*-2-pydaT)](BF_4)$_2$, [**2**]($\mathbf{BF_4}$)$_2$, as the result of the partial chloride dissociation in an aqueous solution of [**1**]($\mathbf{BF_4}$) (see Scheme 1).[16] Here, we describe the isolation and full characterization of this aqua-complex, [**2**]($\mathbf{BF_4}$)$_2$. The synthesis was performed by extraction of the Cl^- ligand from [**1**]($\mathbf{BF_4}$) with an excess of $AgBF_4$ in distilled water at 50 °C, which afforded the expected chiral-at-metal derivative [**2**]-($\mathbf{BF_4}$)$_2$ (see Schemes 1 and 2), as the racemic mixture of the

Scheme 2. Synthesis of the Aqua-Complex [(η^6-*p*-cymene)Ru(OH_2)(κ^2-*N*,*N*-2-pydaT)](BF_4)$_2$, [2**](BF_4)$_2$**

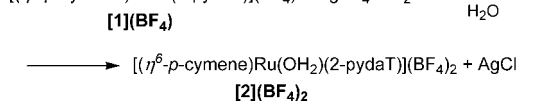

two possible enantiomers, R_{Ru} and S_{Ru}. The yellow solid was obtained in moderate yield (49%) and good analytical purity and is soluble in polar solvents such as water, methanol, and ethanol. The identity of the new compound was confirmed by NMR and IR spectroscopy, FAB+ mass spectrometry, and elemental analysis and molar conductivity.

The ^{1}H NMR spectrum of [**1**]($\mathbf{BF_4}$) in D_2O (18 mM) at room temperature reveals two resonance sets in a 79:21 molar ratio, due to an equilibrium mixture between the chlorido- and aqua-species, $[\mathbf{1}]^+$ and $[\mathbf{2}]^{2+}$ (with D_2O coordinated). Addition of NaCl in excess to this solution led to the suppression of the resonances of [**2**]($\mathbf{BF_4}$)$_2$ demonstrating that [**1**]($\mathbf{BF_4}$) was the major component of the original equilibrium mixture.

The ^{1}H NMR spectrum at room temperature of the isolated aqua-compound [**2**]($\mathbf{BF_4}$)$_2$ in D_2O essentially coincides with that of the minor species in the above aquation-anation equilibrium mixture. Small differences in δ are attributed to a slight pH variation. The spectrum of [**2**]($\mathbf{BF_4}$)$_2$ shows signals for both the *p*-cymene and triazine ligands with the expected pattern; two doublets ascribed to the two diastereotopic methyl groups in the ^{i}Pr entity and an ABCD spin system for the aromatic signals of the *p*-cymene ring are observed, in agreement with an asymmetric coordination environment for the metal center (C1 local symmetry, chirotopic Ru(II) ion). The peaks of the aromatic protons of both ligands appear downfield shifted for $[\mathbf{2}]^{2+}$ relative to those of $[\mathbf{1}]^+$, as expected considering the increase in the cationic charge (Figure 1). The $^{13}C\{^1H\}$ NMR spectrum of $[\mathbf{2}]^{2+}$ is also consistent with the formation of a substitution product at the chloride site of $[\mathbf{1}]^+$, since it shows the same signal pattern as that of $[\mathbf{1}]^+$, although different chemical shifts. Complete assignment of resonances in the ^{1}H and $^{13}C\{^1H\}$ NMR spectra of [**2**]($\mathbf{BF_4}$)$_2$ was performed (see Experimental Section) using 2D NMR experiments such as gCOSY, NOESY, gHSQC and gHMBC.

The FAB+ mass spectrum of compound [**2**]($\mathbf{BF_4}$)$_2$ gave a peak at m/z = 443 consistent with the monocationic parent ion $[M + H\text{-}(BF_4)_2]^+$ according to mass-to-charge ratio and isotopic distribution models. Moreover, the (1:2) electrolyte nature of [**2**]($\mathbf{BF_4}$)$_2$ was corroborated by a molar conductivity

dx.doi.org/10.1021/ic401197a | Inorg. Chem. 2013, 52, 9962−9974

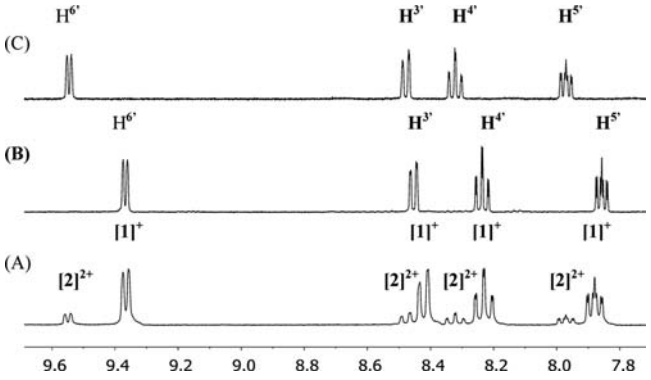

Figure 1. Low field region of the ^{1}H NMR spectra for (A) [**1**]**BF**$_4$ in D_2O at T = 25 °C, showing resonances of the chlorido-complex [**1**]**BF**$_4$ (major) and the aqua-complex [**2**]$^{2+}$ (minor) in a 79:21 ratio at equilibrium (other changes with time were not observed); (B) the same sample after adding NaCl in excess; (C) ^{1}H NMR spectrum for the isolated [**2**](**BF**$_4$)$_2$ product at pH = 3.9.

value of 284 S·cm^2·mol^{-1} measured in CH_3CN at room temperature[20] (see Experimental Section).

Determination of the pK_a Values for [2](BF$_4$)$_2$. In order to establish the pH range for the existence of the aqua-complex [**2**](**BF**$_4$)$_2$, the pK_a values were determined from the variation of the absorbance spectra with pH, Figure 2.

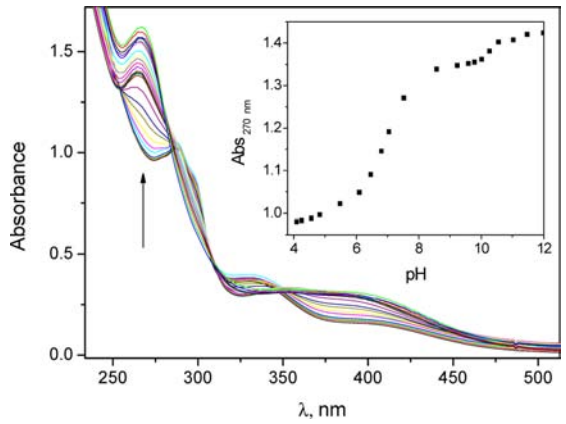

Figure 2. Absorbance spectra of a 9.0 × 10^{-5} M solution of [**2**](**BF**$_4$)$_2$, I = 2.5 mM and T = 25 °C, recorded in the pH 4−12 range (arrow sense). Inset: pH effect on the [**2**](**BF**$_4$)$_2$ absorbance at λ = 270 nm.

Figure 2 (inset) shows the pH effect on the absorbance at λ = 270 nm; the fitting of the resulting curve to the Henderson−Hasselbalch equation[21] yielded the values pK_{a1} = 7.0, related to the deprotonation of the coordinated aquo ligand to give the hydroxido derivative [**3**](**BF**$_4$) (Scheme 1), and pK_{a2} = 10.3, related to an ionizable function of the coordinated 2-pydaT ligand in [**2**](**BF**$_4$)$_2$, most likely one of the −NH_2 groups. pK_a values of 7.2 and 7.7 have been reported for the coordinated water molecule in [(η^6-*p*-cymene)Ru(bipy)(H_2O)]$^{2+}$, and [(η^6-bip)Ru(en)(H_2O)]$^{2+}$ (bipy = 2,2′-bipyridine, bip = biphenyl, en = ethylenediamine), respectively.[18,22] Therefore, the reactivity experiments were performed at pH ≤ 7 to ensure the presence of the aqua-complex in solution, since ruthenium hydroxido complexes are kinetically more inert and hence biologically less active.[14]

Reactivity of [2](BF$_4$)$_2$ with 9-MeG. The reaction between [**2**](**BF**$_4$)$_2$ (10 mM) and 9-methylguanine, **9-MeG** (20 mM) was monitored by ^{1}H NMR in D_2O at T = 25 °C and pH = 7.0 (Figure 3). The resulting spectra allowed us to observe the gradual formation of [(η^6-*p*-cymene)Ru(2-pydaT)(*N*7-9-MeG)]$^{2+}$, [**4**]$^{2+}$ (Figure 4), over time (74% after 24 h and 88% after 48 h).

The coordination of **9-MeG** to the Ru(II) ion is assumed to occur through N7, the potential binding site in DNA (see confirmation below in the X-ray structure). The ^{1}H NMR singlet (1H) at 6.81 ppm is attributed to H$^{8''}$ of the coordinated nucleobase, **9-MeG** (see Figure 4 for selected numbering). The high-field shift observed for this signal relative to that of free **9-MeG** ($\Delta\delta$ = 0.92 ppm), in line with the values reported for other Ru(II)-guanine adducts,[23−25] most likely stems from the proximity of an aromatic ring of 2-pydaT which strongly shields H$^{8''}$ upon coordination. In fact, a CH−π interaction between this hydrogen and the pyridine ring is observed in the molecular structure of [**4**](**PF**$_6$)$_2$ (vide infra). As expected, just one set of signals is observed for the racemic mixture of enantiomers (R_{Ru}, S_{Ru}) [(η^6-*p*-cymene)Ru(2-pydaT)(*N*7-9-MeG)]$^{2+}$, [**4**]$^{2+}$ (Figure 3).

The reaction between [**2**](**BF**$_4$)$_2$ and **9-MeG** monitored at pH = 9.0 and T = 25 °C showed a slower evolution, with 41% formation of [**4**]$^{2+}$ after 24 h, revealing the more inert nature of the hydroxido complex [**3**]$^+$ (Scheme 1), allegedly formed under these conditions. Furthermore, two additional reactions between [**1**](**BF**$_4$) (10 mM) and **9-MeG** (20 mM) were monitored by ^{1}H NMR in D_2O at pH = 7, T = 25 °C, both in the absence and in the presence of NaCl (0.1 M), yielding [**4**]$^{2+}$ with different conversion percentages as deduced from NMR integration (Figures 1SI-A and 2SI-B, Supporting Information). Thus, the conversion starting from [**1**](**BF**$_4$) after 24 h was 38% in the presence of NaCl, and 63% in the absence of NaCl, compared to 74% starting from [**2**](**BF**$_4$)$_2$ in the absence of NaCl (see above). These figures reveal the lower reactivity of [**1**](**BF**$_4$) compared to [**2**](**BF**$_4$)$_2$ and the concomitant inhibition effect of the Cl^- anions. Hence, we postulate that the aqua product, [**2**](**BF**$_4$)$_2$, is the active species, and that aquation is a prerequisite for the reaction of [**1**](**BF**$_4$) with **9-MeG**.

Lastly, [**1**](**BF**$_4$) was reacted in water with **9-MeG** at 37 °C in an Schlenk tube, to produce the nucleobase derivative [(η^6-*p*-cymene)Ru(2-pydaT)(*N*7-9-MeG)]$^{2+}$, [**4**]$^{2+}$ which was isolated as the corresponding PF_6^- salt, [**4**](**PF**$_6$)$_2$, by addition of NH_4PF_6. The complex was fully characterized by spectroscopy and X-ray diffraction measurements. The ^{1}H NMR spectrum of the resulting crude solid in D_2O showed resonances assigned to the expected complex but also traces of [**1**]$^+$ (5%) and [**2**]$^{2+}$ (7%) (see Figure 2SI, Supporting Information). To date, only a few Ru(II) arene derivatives with **9-EtG** (9-ethylguanine)[26,27] or **9-MeG**[28] have been prepared by similar procedures, including the related complexes [(η^6-tha)Ru(bipy)(*N*7-9-EtG)](PF$_6$)$_2$ and [(η^6-tha)Ru(bipy(OH)O)(*N*7-9-EtG)](PF$_6$), where tha = tetrahydroanthracene, bipy = 2,2′-bipyridine.

X-ray Diffraction of [(η^6-p-cymene)RuCl(κ^2-N,N-2-pydaT)](PF$_6$), [1](PF$_6$) and [(η^6-p-cymene)Ru(κ^2-N,N-2-pydaT)(N7−9-MeG)](PF$_6$)$_2$, [4](PF$_6$)$_2$. Single crystals of both [(η^6-*p*-cymene)-RuCl(κ^2-*N*,*N*-2-pydaT)](PF$_6$), [**1**](**PF**$_6$) and [(η^6-*p*-cymene)-Ru(κ^2-*N*,*N*-2-pydaT)(*N*7-9-MeG)](PF$_6$)$_2$, [**4**](**PF**$_6$)$_2$, suitable for X-ray diffraction, were obtained from the same sample after 10 days ([**1**](**PF**$_6$)) and two months ([**4**](**PF**$_6$)$_2$), by slow diffusion of diethylether into a methanol/water solution of the impure nucleobase derivative [(η^6-*p*-cymene)Ru(9-MeG)(κ^2-*N*,*N*-2-pydaT)](PF$_6$)$_2$, [**4**](**PF**$_6$)$_2$, which according to NMR

dx.doi.org/10.1021/ic401197a | Inorg. Chem. 2013, 52, 9962−9974

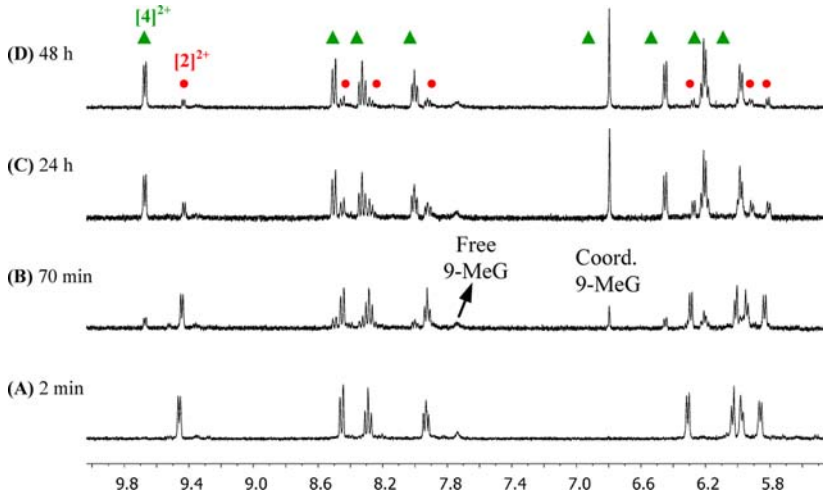

Figure 3. Low field region of the ^{1}H NMR spectra in D_2O for the reaction between $[\mathbf{2}](\mathbf{BF_4})_2$ and **9-MeG** (1:2, 10 mM, pH = 7) after: (A) 2 min; (B) 70 min; (C) 24 h; (D) 48 h. Labels key are green triangle = $[\mathbf{4}]^{2+}$; red circle = $[\mathbf{2}]^{2+}$. Signals labeled as $[\mathbf{2}]^{2+}$ show weighed average chemical shifts for the equilibrium mixture between $[\mathbf{2}]^{2+}$ and $[\mathbf{3}]^{+}$.

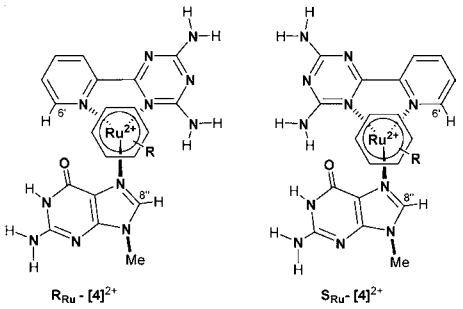

Figure 4. Structures of enantiomers R_{Ru} and S_{Ru} of complex $[(\eta^6\text{-}p\text{-cymene})\mathrm{Ru}(2\text{-pydaT})(N7\text{-}9\text{-MeG})]^{2+}$, $[\mathbf{4}]^{2+}$. Ligand priority sequence: arene > N(triazine) > N(guanine) > N(pyridine).

analysis contained a small fraction (5%) of $[(\eta^6\text{-}p\text{-cymene})\mathrm{RuCl}(\kappa^2\text{-}N,N\text{-}2\text{-pydaT})]^{+}$, $[\mathbf{1}]^{+}$ (Figure 2SI, Supporting Information). The ORTEP diagrams are shown in Figure 5, the selected bond lengths and angles with estimated standard deviations are listed in Table 1, and the relevant crystallographic parameters are given in the Supporting Information (Tables 3SI and 8SI). Both products crystallize in the $P\bar{1}$ space group of the triclinic system. In the case of $[\mathbf{1}](\mathbf{PF_6})$, the asymmetric unit contains a single cationic complex plus a PF_6^- counterion and a hydration water molecule, while the unit cell comprises two enantiomeric metal complexes (R_{Ru} and S_{Ru}), along with two counterions and two hydration water molecules. On the other hand, the asymmetric unit of compound $[\mathbf{4}](\mathbf{PF_6})_2$ consists of four anions plus two independent (R_{Ru}) complex cations (A and B) which show slight differences between them (see Table 1). In the corresponding unit cell, eight counterions and four cations, two R_{Ru} and two S_{Ru}, are present. The metal complexes adopt the classical pseudo-octahedral three-legged piano-stool geometry, with the arene ring displaying a π-bonded η^6 coordination mode. Moreover, the 2-pydaT ligand assumes a chelate-bidentate coordination fashion (κ^2-*N*,*N*), while either the chloride ion or the **9-MeG** ligand resides in the third leg of the stool. It is interesting to point out that both $[\mathbf{1}](\mathbf{PF_6})$ and $[\mathbf{4}](\mathbf{PF_6})_2$ display similar features as those of the related specimen $[(\eta^6\text{-benzene})\mathrm{RuCl}(\kappa^2\text{-}N,N\text{-}2\text{-pydaT})](\mathrm{BF_4})$, $[\mathbf{1b}](\mathbf{BF_4})$ reported recently by us[16] (see Table 1 for comparison). Thus, the Ru(1)−N(1)

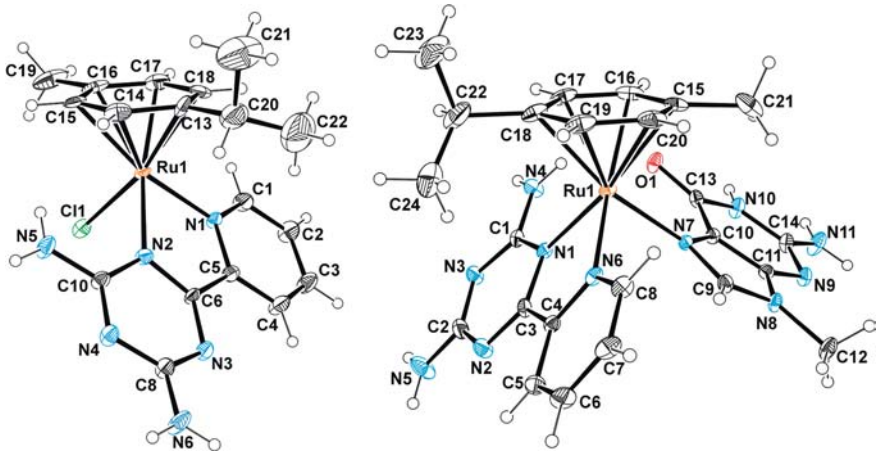

Figure 5. ORTEP diagrams for the molecular structure of compounds $[\mathbf{1}](\mathbf{PF_6})$ and $[\mathbf{4}](\mathbf{PF_6})_2$. For the sake of clarity, only enantiomers $\boldsymbol{S_{Ru}}$ for $[\mathbf{1}](\mathbf{PF_6})$ and $\boldsymbol{R_{Ru}}$ for $[\mathbf{4}](\mathbf{PF_6})_2$ are shown. PF_6^- counterions and solvent molecules are omitted in both diagrams. Thermal ellipsoids are shown at the 50% probability.

dx.doi.org/10.1021/ic401197a | *Inorg. Chem.* 2013, 52, 9962−9974

Table 1. Selected Bond Lengths (Å) and Angles (°) for [(η^6-*p*-cymene)RuCl(κ^2-*N*,*N*-2-pydaT)](PF_6), [**1**](PF_6), [(η^6-benzene)RuCl(κ^2-*N*,*N*-2-pydaT)](BF_4), [**1b**](BF_4), and [(η^6-*p*-cymene)Ru(κ^2-*N*,*N*-2-pydaT)(*N*7-9-MeG)](PF_6)$_2$, [**4**](PF_6)$_2$

distances/angles	[**1**](PF_6)	distances/angles	[**1b**](BF_4)[16]	distances/angles	[**4**](PF_6)$_2$ **A** and **B**
Ru−arene (centroid)[a]	1.688	Ru−arene (centroid)	1.673	Ru(1)−centroid	1.691
				Ru(2)−centroid	1.702
Ru(1)−Cl(1)	2.406(2)	Ru(1)−Cl(2)	2.393(3)	Ru(1)−N(7)	2.130(3)
				Ru(2)−N(18)	2.133(3)
Ru(1)−N(1)py	2.092(6)	Ru(1)−N(6)py	2.07(1)	Ru(1)−N(6)py	2.097(4)
				Ru(2)−N(17)py	2.088(4)
Ru(1)−N(2)tz	2.116(5)	Ru(1)−N(1)tz	2.100(9)	Ru(1)−N(1)tz	2.135(3)
				Ru(2)−N(12)tz	2.137(3)
C(8)−N(6)	1.312(9)	C(1)−N(4)	1.321(16)	C(2)−N(5)	1.314(6)
				C(32)−N(16)	1.328(6)
C(10)−N(5)	1.329(9)	C(2)−N(5)	1.301(16)	C(1)−N(4)	1.318(6)
				C(31)−N(15)	1.317(6)
N(1)−Ru(1)−N(2)	76.8(2)	N(6)−Ru(1)−N(1)	76.0(4)	N(1)−Ru(1)−N(6)	76.61(13)
				N(12)−Ru(2)−N(17))	76.40(13)
N(1)−Ru(1)−Cl(1)	85.61(17)	N(6)−Ru(1)−Cl(2)	88.8(3)	N(6)−Ru(1)−N(7)	86.49(13)
				N(17)−Ru(2)−N(18)	87.65(13)
N(2)−Ru(1)−Cl(1)	84.44(16)	N(1)−Ru(1)−Cl(2)	84.2(3)	N(1)−Ru(1)−N(7)	87.50(13)
				N(12)−Ru(1)−N(18)	87.19(13)

[a]Mercury 3.0.

(pyridine) distances are considerably shorter than the Ru(1)−N(2) (triazine) lengths in the three complexes in agreement with the lower basicity of the second heterocycle. The triazine ring of 2-pydaT deviates slightly from planarity in all the cases. On the other hand, the $-NH_2$ groups present trigonal planar arrangements with short C-NH_2 distances in every specimen. The Ru−Cl bond distance is 2.406(2) Å for [**1**](PF_6), whereas the Ru−N (9-MeG) lengths are 2.130(3) Å (A) and 2.133(3) Å (B) for [**4**](PF_6)$_2$. Finally, the Ru-arene (centroid) distances are 1.688 Å for [**1**](PF_6), and 1.691 Å (A) and 1.701 Å (B) for [**4**](PF_6)$_2$, while the bite angles of the five-membered chelate rings are 76.8(2)° for [**1**](PF_6), and 76.61(13)° (A) and 76.40(13)° (B) for [**4**](PF_6)$_2$.

Interestingly, in the case of [**4**](PF_6)$_2$ there are two intramolecular H-bonding interactions between the **9-MeG** and the metallic fragment [(η^6-*p*-cymene)Ru(2-pydaT)]$^{2+}$ (see Table 2 and Figure 17SIA). These contacts involve the O atom

Table 2. Intramolecular H-Bonding Parameters for [**4**](PF_6)$_2$

H-bonding	D---A (Å)	H---A (Å)	D−H (Å)	α (deg)
N(4)H(4B)---O(1)	2.753	2.190	0.861	122.72
N(15)H(15B)---O(2)	2.753	2.135	0.860	128.39
C(16)H(16)---O(1)	3.043	2.441	0.929	122.45
C(46)H(46)---O(2)	2.996	2.402	0.930	121.62

of **9-MeG**, as the acceptor, and both the $-NH_2$ group of 2-pydaT [N(4)H(4B)---O(1) for (A) and N(15)H(15B)---O(2) for (B)] and a C−H of the *p*-cymene [C(16)H(16)---O(1) for (A) and C(46)H(46)---O(2) for (B)], as the donors. There is also a CH−π interaction between H(9) of **9-MeG** and the pyridine ring. All these weak interactions reinforce the linkage of the metal fragment with **9-MeG** as a model for DNA. In particular, the aforementioned H-bonding contacts introduce a certain degree of selectivity for guanine versus adenine, which is endowed with a $-NH_2$ group on C6 instead of the C═O and therefore exerts repulsion.

The 3D crystal structures of [**1**](PF_6) and [**4**](PF_6)$_2$ are held mainly by H-bonding interactions and are briefly commented on in the Supporting Information.

Interaction of [2](BF_4)$_2$ or [1](BF_4) with 2′-Deoxyguanosine 5′-Monophosphate (5′-dGMP) or 2′-Deoxyadenosine 5′-Monophosphate (5′-dAMP). An in-depth analysis of the binding mechanism of [**2**](BF_4)$_2$ to DNA was performed by reacting the aqua-complex with two different nucleotides: (2′-deoxyguanosine 5′-monophosphate, **5′-dGMP**, or 2′-deoxyadenosine 5′-monophosphate, **5′-dAMP**). The reactions were followed by ^{1}H and ^{31}P{^{1}H} NMR, and UV−vis and kinetic experiments. First of all, the reaction between [**2**](BF_4)$_2$ and **5′-dGMP** in D_2O was studied in the absence of NaCl at an adjusted pH value of 7.0 by NMR. The evolution of the ^{1}H and ^{31}P{^{1}H} NMR spectra are consistent with the formation of two nucleotido-derivative pairs ([**5a**], [**5b**]) and ([**5c**], [**5d**]) in two consecutive steps (Figures 3SI and 4SI, Supporting Information). We propose that the two (Ru−O(PO_3)-dGMP) diastereomers, [**5a**] and [**5b**], are initially yielded in a 1:1 molar ratio as the result of water displacement in the aqua-complex, [**2**]$^{2+}$. Then, we assume that intermediates [**5a**] and [**5b**] transform into the more stable Ru−N7-dGMP linkage diastereomers, [**5c**] and [**5d**], which are obtained in a 1:1 proportion as well (see Figure 6). In conclusion, we suggest that [**5a**] and [**5b**] are kinetic isomers and [**5c**] and [**5d**] are thermodynamic products.

Similarly, the reaction between [**1**](BF_4) and **5′-dGMP** was carried out in an NMR tube in D_2O in the presence of NaCl (I = 0.1 M) and pH = 7.0. The evolution of the corresponding ^{1}H and ^{31}P{^{1}H} NMR spectra is shown in Figures 5SI and 6SI, Supporting Information and is consistent with the formation of [**2**]$^{2+}$ and then the two nucleotido-derivative pairs ([**5a**], [**5b**]) and ([**5c**], [**5d**]) in two consecutive steps. However, in this case [**2**]$^{2+}$ and the pair [**5a**], [**5b**] are observed as minor species along the whole reaction. Moreover, the process is slower and does not go to completion.

Despite yielding similar results, certain differences are deduced from the comparison of the reactions between **5′-dGMP** and both [**2**]$^{2+}$ (in the absence of Cl^-) and [**1**]$^+$ (in the

dx.doi.org/10.1021/ic401197a | *Inorg. Chem.* 2013, 52, 9962−9974

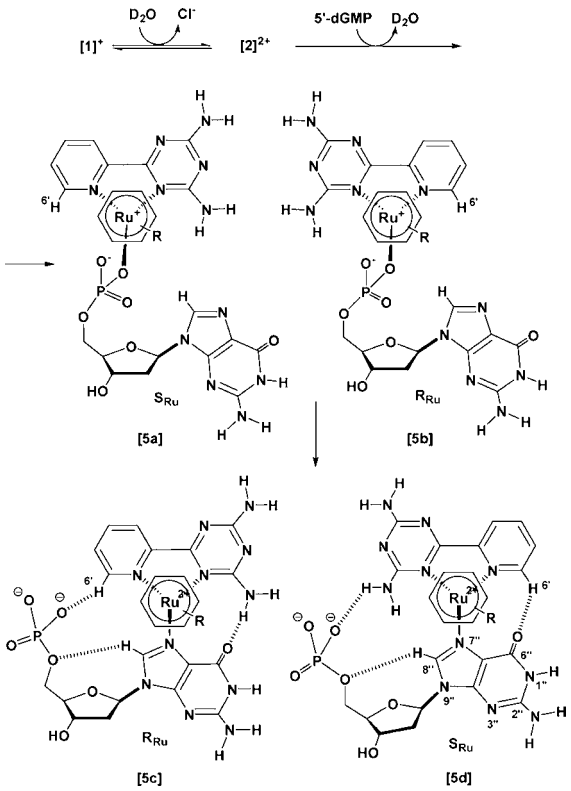

Figure 6. Structure of the Ru−O(PO_3)-dGMP intermediates, [**5a**] and [**5b**], and the corresponding Ru−N7-dGMP isomers, [**5c**] and [**5d**], with their respective absolute configuration. Possible H-bonds have been depicted for [**5c**] and [**5d**].

presence of Cl^-): (i) The reaction with $[\mathbf{1}]^+$ reaches equilibrium and does not evolve to completion, even after 14 days, whereas the reaction with $[\mathbf{2}]^{2+}$ is almost completed after 3 days; (ii) for reaction with $[\mathbf{1}]^+$, isomers [**5a**] and [**5b**] are observed as minor species over the whole reaction, whereas for the reaction with $[\mathbf{2}]^{2+}$, isomers [**5a**] and [**5b**] are initially observed as the major species (10 min) and afterward they vanish steadily, transforming into [**5c**] and [**5d**]. We propose that starting from $[\mathbf{1}]^+$ the formation of [**5a**] and [**5b**] is slower (in the presence of Cl^-) than starting from $[\mathbf{2}]^{2+}$ (in the absence of Cl^-) because the substitution step takes place over $[\mathbf{2}]^{2+}$ regardless of the starting material used.

Then, $[\mathbf{2}](\mathbf{BF_4})_2$ was reacted with 5′-deoxyguanylic acid, **5′-dGMP**, at a lower pH value (pH = 2.6), in which the phosphate group could be protonated to get additional support for the structures proposed for [**5a**], [**5b**], [**5c**], and [**5d**]. The low field region of the ^{1}H NMR spectrum for $[\mathbf{2}](\mathbf{BF_4})_2$ is shown in Figure 7SI, Supporting Information, along with the corresponding spectra for the reaction with **5′-dGMP** (1:1, 5 mM, pH = 2.6) at several reaction times. Under these conditions, only the Ru-*N7*-dGMP isomers similar to [**5c**] and [**5d**] are formed. It is noteworthy that the corresponding (Ru−O(PO_3)-dGMP) species are not observed at low pH, possibly as a consequence of semiprotonation of the phosphate group.

The reaction between $[\mathbf{2}](\mathbf{BF_4})_2$ and **5′-dAMP** was followed by ^{1}H and ^{31}P{^{1}H} NMR in D_2O at pH = 7.0 and T = 25 °C, but no reaction was clearly observed, even after 15 days (see Figure 8SI, Supporting Information). Sadler et al. have reported that the pH-dependent reaction of 5′-**dAMP** with $[(\eta^6$-bip)Ru(en)Cl]$^+$, where bip = biphenyl, gives rise to the phosphate-bound adduct Ru−O(PO_3)AMP as the only product in equilibrium with the precursor (at pH = 7.2), indicating that repulsive interactions with the C6 $-NH_2$ group avoid the coordination through N7 or N1 in adenine.[19]

UV−vis Kinetic Experiments. To corroborate the reaction mechanism put forward on the basis of NMR measurements and evaluate the reaction parameters, additional UV−vis kinetic experiments with either $[\mathbf{1}](\mathbf{BF_4})$ or $[\mathbf{2}](\mathbf{BF_4})_2$ and **5′-dGMP** were carried out. $[\mathbf{1}](\mathbf{BF_4})$ undergoes reaction with **5′-dGMP** in two consecutive steps (Figure 9SI, Supporting Information), the kinetic curve fitting to a biexponential function with $k_a = (9.5 \pm 0.1) \times 10^{-4}$ s^{-1} and $k_2 = (1.9 \pm 0.2) \times 10^{-4}$ s^{-1}. The first branch shows a decrease in the absorbance intensity at λ = 350 nm due to the aquation process. The corresponding rate contant, k_a, is comparable to that obtained for the aquation of $[\mathbf{1}](\mathbf{BF_4})$ in water ($(7.5 \pm 0.2) \times 10^{-4}$ s^{-1})[16] to yield $[\mathbf{2}](\mathbf{BF_4})_2$, whereas k_2 is the formation rate constant of the $[\mathbf{2}](\mathbf{BF_4})_2$/**5′-dGMP** (Ru−N7) adduct ([**5c**] and [**5d**]) (Figure 7). This is in accordance with the results of the NMR experiments.

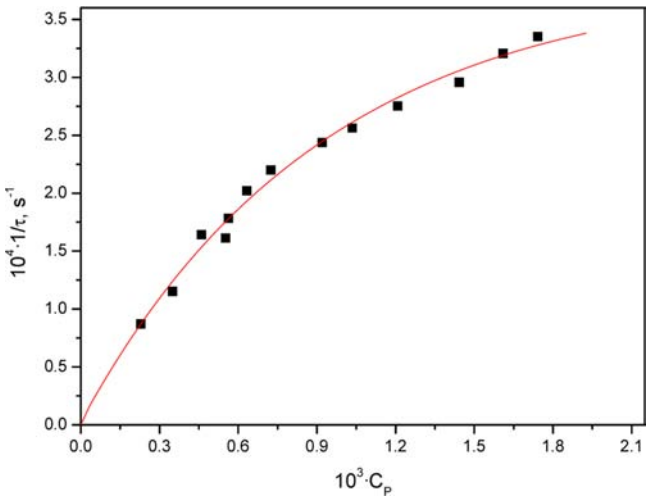

Figure 7. Analysis according to eq 2 of the dependence of the reciprocal relaxation time on C_P for $[\mathbf{2}](\mathbf{BF_4})_2$ /**5′-dGMP** system. I = 2.5 mM, pH = 6.0 and T = 25 °C.

The scheme of Figure 6 is also confirmed by UV−vis kinetic experiments for the synthetic $[\mathbf{2}](\mathbf{BF_4})_2$ and **5′-dGMP** system (now denoted as D/P, D being the $[\mathbf{2}](\mathbf{BF_4})_2$ complex and P the nucleotide). The experiments were performed under pseudo-first-order conditions, with $C_P \geq 10C_D$. The kinetic curves were monoexponential (Figure 10SI, Supporting Information), and the plot of the time constants ($1/\tau$) versus **5′-dGMP** concentration (C_p) passes through the origin and tended to a plateau (Figure 7). This behavior is in agreement with the multistep mechanism:

$$P + D \overset{K_1}{\rightleftharpoons} PD_I \overset{k_2}{\rightarrow} PD_{II} \quad (1)$$

On this basis, the $1/\tau$ versus C_P data-pairs were fitted to eq 2,

$$1/\tau = K_1 \times k_2 C_P/(1 + K_1 C_P) \quad (2)$$

These results can be interpreted assuming (i) the $[\mathbf{2}](\mathbf{BF_4})_2$ species reacts quickly with **5′-dGMP** to form the PD_I complex, K_1 being the equilibrium constant of this step, and (ii) the PD_I complex converts into PD_{II} in a second irreversible, unimolecular step, k_2 being the rate-determining constant. Table 3 collects the values obtained for the rate constant k_2, and

dx.doi.org/10.1021/ic401197a | Inorg. Chem. 2013, 52, 9962−9974

Table 3. Kinetic Constants, k_i, and Apparent Binding Constant, K_i, for the $[2](BF_4)_2$/5′-dGMP (k_2 and K_1) and $[2](BF_4)_2$ /CT-DNA Systems (k_1', k_{-1}', k_2', K_1', and K_1''), I = 2.5 mM, pH = 6.0 and T = 25 °C

	10^{-4} k_1' ($M^{-1}s^{-1}$)	10^{2} k_{-1}' (s^{-1})	10^{-2} K_1 (M^{-1})	10^{-6} K_1' (M^{-1})	10^{-3} K_1''	10^{4} k_2 (s^{-1})	10^{4} k_2' (s^{-1})
5′-dGMP			9.3 ± 0.3			3.2 ± 0.6	
CT-DNA	2.2 ± 0.3	1.4 ± 0.4		1.6 ± 0.1	1.7 ± 0.3		1.5 ± 0.01

the equilibrium constant K_1. The partial and overall orders of reaction were determined by the initial rate method under both equimolar, $C_P = C_D$, and pseudo-first-order ($C_P \gg C_D$) conditions. Figure 11SI-A, Supporting Information shows the $\ln(\text{Abs}/t)_0$ versus $\ln C_P$ plot at 300 nm; the slope yielded the overall order $n = 2$. The slope of Figure 11SI-B corresponds to **5′-dGMP** and gave partial kinetic order $\alpha = 1$. Therefore, the $[2](BF_4)_2$ partial order must be $\beta = 1$, in good agreement with the expectations.

These results are consistent with those obtained by $^{31}P\{^1H\}$ NMR (Figure 4SI, Supporting Information) and reveal that PD_I corresponds to the complex formed between the metal center of $[2](BF_4)_2$ and the phosphate group of **5′-dGMP**, (diastereoisomers [**5a**] and [**5b**]). Metal ions have been shown to previously interact with the phosphate oxygen atoms,[29] whereas PD_{II} is the covalent complex Ru−N7-dGMP (diastereoisomers [**5c**] and [**5d**]) (Figure 3SI, Supporting Information).

The stopped-flow experiments gave no kinetic curves, revealing that the fast reaction between the O-phosphate and $[2](BF_4)_2$ is faster than milliseconds; this outcome was also expected, since the interaction between phosphate groups and divalent cations is a very fast process.[29,30]

Interaction of $[2](BF_4)_2$ with CT-DNA. The interaction of $[2](BF_4)_2$ with CT-DNA was studied by UV−vis kinetic experiments, CD and viscosity measurements, and thermal denaturation assays. Cytotoxicity assays were also performed.

UV−vis Kinetic Experiments. Unlike the interaction of $[2](BF_4)_2$ with **5′-dGMP**, in which only a single rate constant (k_2) was determined (see above), two different processes over different time scales (fast and slow) have been detected in the presence of CT-DNA. The stopped flow technique with absorbance detection was used to study the fast reaction between $[2](BF_4)_2$ (D) and CT-DNA (P) under pseudo-first-order conditions ($C_P \geq 10C_D$); as an example, a kinetic curve is shown in Figure 12SI, Supporting Information. The reciprocal of the relaxation time, $1/\tau_f$, evaluated from analysis of the averaged curves, was plotted versus DNA concentration, yielding a straight line (Figure 8). The apparent binding behavior agrees well with a one-step mechanism, defined by the reaction:

$$P + D \underset{k_{-1}'}{\overset{k_1'}{\rightleftharpoons}} PD' \tag{3}$$

and governed by the kinetic equation:

$$\frac{1}{\tau_f} = k_{-1}' + k_1' C_P \tag{4}$$

The slope (k_1') over the intercept (k_{-1}') ratio affords the apparent binding constant, $K_1' = k_1'/k_{-1}'$. Table 3 lists the rate constants k_1', k_{-1}', and equilibrium constant K_1' obtained for the $[2](BF_4)_2$/DNA system, compared with those for the $[2](BF_4)_2$/5′-**dGMP** system. The value $K_1' = (1.6 \pm 0.1) \times 10^6$ M^{-1} is similar to the intrinsic intercalation constant ($K = 2.5 \times 10^6$ M^{-1}, T = 23 °C, I = 0.015 M)[31] for ethidium bromide/DNA, revealing that the process observed by stopped flow

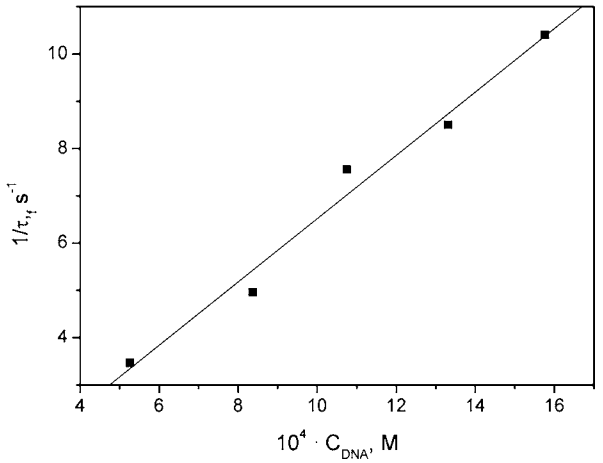

Figure 8. Dependence of the reciprocal fast relaxation time on the DNA concentration for the $[2](BF_4)_2$ /CT-DNA system, I = 2.5 mM, pH = 6.0 and T = 25 °C.

corresponds to intercalation of the planar moiety 2-pydaT into DNA. The kinetic constants for the $[2](BF_4)_2$/DNA system, $k_1' = (2.2 \pm 0.3) \times 10^4$ M^{-1} s^{-1} and $k_{-1}' = 0.014 \pm 0.004$ s^{-1} differ, for example, from those of intercalation of the mutagen proflavine into CT-DNA at I = 0.1 M,[32] with formation and dissociation rate constants $k_1 = 4.3 \times 10^7$ M^{-1} s^{-1} and $k_{-1} = 6.8 \times 10^2$ s^{-1}, respectively. For $[2](BF_4)_2$, the lower rates of formation of the intercalated complexes support that intercalation of 2-pydaT is more hindered than the planar proflavine (acridine-3,6-diamine). The behavior of the dissociation rate constant is quite interesting; in fact, the longer the intercalated species remain inside the DNA, the more efficient the drugs are,[33] thus favoring $[2](BF_4)_2$ relative to proflavine ($k_{-1}' < k_{-1}$).

Like for the $[2](BF_4)_2$/5′-**dGMP** system (Figure 10SI, Supporting Information), a slow single exponential is observed for the interaction between $[2](BF_4)_2$ and CT-DNA (Figure 13SI, Supporting Information). A kinetic study under pseudo-first-order conditions gave the partial kinetic order $\alpha = 1.01 \pm 0.02$ (Figure 14SI, Supporting Information). The $1/\tau_s$ versus C_P plot corresponding to the slow effect yielded a constant value k_2' (Table 3). A nonlinear behavior was expected from the $1/\tau_s$ versus C_P plot, similar to the $[2](BF_4)_2$/5′-**dGMP** system (Figure 7). However if, as occurs here, K_1' is larger than K_1, then eq 2 (with K_1, k_2, and τ replaced by K_1', k_2', and τ_s, respectively) reduces to $1/\tau_s = k_2'$, concurrent with the DNA-independent concentration constant. For the slow step k_2', a two-step mechanism can be proposed, formally similar to that for $[2](BF_4)_2$ /5′-**dGMP** in eq 1.

$$P + D \overset{K_1'}{\rightleftharpoons} PD' \overset{k_2'}{\rightarrow} PD_{II}' \tag{5}$$

The data of Table 3 reveal that PD′ (eq 5) and PD_I (eq 1) are endowed with distinct features. The apparent constant K_1' is 3 orders of magnitude higher than K_1, denoting two different processes; PD′ is an intercalated complex, whereas PD_I is a

dx.doi.org/10.1021/ic401197a | Inorg. Chem. 2013, 52, 9962−9974

complex formed between the metal of $[2](BF_4)_2$ and the phosphate group. Therefore, it can be assumed reasonably that the formation of PD′ takes place in two steps with different equilibrium constants, K_1 and K_1'', in accordance with the reaction scheme:

$$P + D \overset{K_1}{\rightleftharpoons} PD_I \overset{K''_1}{\rightleftharpoons} PD' \overset{k_2'}{\rightarrow} PD_{II}' \quad (6)$$

The fast effect corresponds to formation of PD′, whose apparent constant K_1' is the combination of two consecutive steps with apparent constants K_1 and K_1''; that is, Ru(II) binds very fast to the DNA phosphate group in $[2](BF_4)_2$ (not detected by stopped flow) forming the PD_I complex, similar to that observed with ^1H and $^{31}P\{^1H\}$ NMR measurements for $[2](BF_4)_2$/**5′-dGMP**. In a second fast step (observed with stopped flow), PD_I transforms into the intercalated PD′, from which the bifunctional covalent-intercalated PD_{II}' complex is formed. The $K_1'' = 1.7 \times 10^3$ value, inferred from the K_1 and K_1' constants (Table 3), is (roughly) twice the K_1' value, which supports the formation of PD′ from PD_I.

Covalent binding occurs between the metal and the N7 site of the guanine DNA residues, consistent with the close k_2 and k_2' values obtained for $[2](BF_4)_2$/**5′-dGMP** and $[2](BF_4)_2$/CT-DNA, respectively (Table 3) and the NMR results, which confirm that $[2](BF_4)_2$ only reacts with **5′-dGMP** and not with 5′-dAMP. Lastly, k_2' is twice lower than the k_2 value corresponding to the covalent binding for $[2](BF_4)_2$/**5′-dGMP** system, indicating that the intercalation hinders the formation of the covalent binding.

It shall be demonstrated below that the two types of interaction, covalent and intercalated, are present concurrently in PD_{II}', providing this complex with bifunctional features; 2-pydaT intercalates between the DNA base-pairs, whereas ruthenium binds to the N7 site of guanine. Despite being 2-pydaT also present in $[1](BF_4)$, it does not intercalate into CT-DNA.[16] A notable difference between $[1](BF_4)$ and $[2](BF_4)_2$ is that the intermediate PD_I (Ru−O(PO_3)) is formed only as a minor species from the chloride-complex. These observations permit one to conclude that not only is the aqua-complex $[2](BF_4)_2$ prone to intercalate into DNA, but also its metal center is able to interact with the DNA phosphate group forming PD_I; this, in turn, may act also as an intermediate prior to forming the intercalated PD′ and the bifunctional intercalated-covalent PD_{II}' (eq 6). These features confer $[2](BF_4)_2$ a deal of pharmacological promise, as shown below in the biological assays.

CD Measurements. The circular dichroism spectra recorded during the titrations evince an induced circular dichroism (ICD) effect in the VIS range and perturbations in the UV region (Figure 9). In the UV region, the molar ellipticity of both negative and positive bands of the CT-DNA spectra decreased as the C_D/C_P ratio rose, displaying a 20 nm shift to red; this behavior is characteristic of intercalation. Three new ICD bands appeared, two positive and a negative weaker one. As $[2](BF_4)_2$ has no intrinsic CD signal, the ICD bands demonstrate the formation of the $[2](BF_4)_2$/CT-DNA complex.[34] Two isodichroic points emerged at 350 and 395 nm. Figure 9 (inset) shows the variation of the molar ellipticity at $\lambda = 435$ nm with the C_D/C_P ratio. A first branch increased up to $C_D/C_P \sim 1$, reaching a maximum from which a second complex is formed. The complexes observed by CD at $C_D/C_P > 1$ normally are external provided that D is prone to form aggregates.[35] The X-ray data have shown that in the solid state

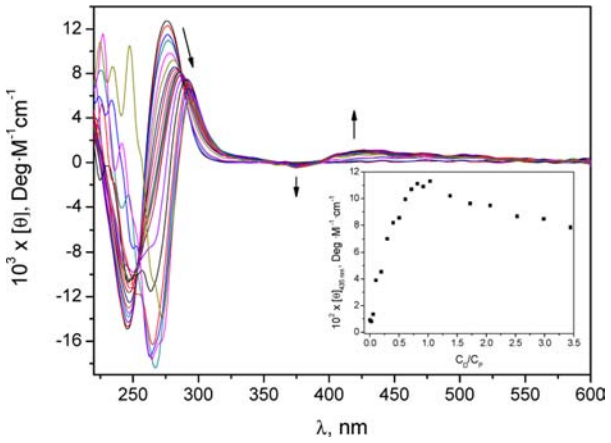

Figure 9. CD spectra for the $[2](BF_4)_2$/CT-DNA system $C_P = 1.03 \times 10^{-4}$ M, $C_D/C_P = 0 - 3.5$ (arrow sense). Inset: Dependence of the molar ellipticity at $\lambda = 435$ nm on the C_D/C_P ratio. $I = 2.5$ mM, pH = 6.0 and $T = 25$ °C.

formation of dimers between enantiomers is feasible (Figure 16SI, Supporting Information). Even though such dimers have not been observed in solution in the absence of DNA, in the presence of DNA the partially intercalated enantiomer may act as a scaffold, thus promoting the binding to the other enantiomer to yield dimers similar to those observed in the solid state.

Viscosity. The CD conclusions were corroborated by viscosity measurements. The L/L_0 versus C_D/C_P plot, L and L_0 being the DNA contour length in the sample and alone, respectively (Figure 10), shows an increase in the DNA contour length, reaching a plateau; intercalation of a dye between the DNA base-pairs causes local unwinding with elongation of the double helix.[36]

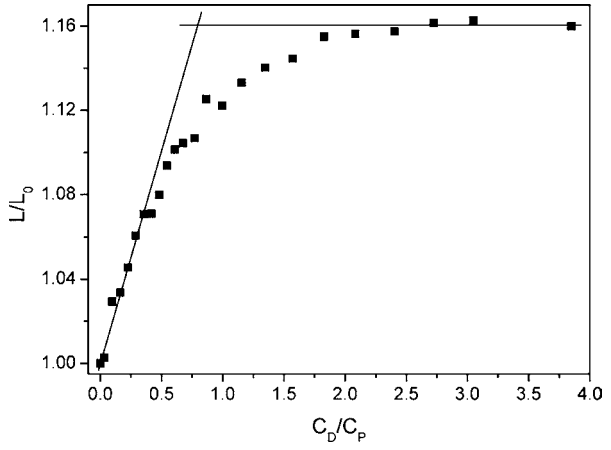

Figure 10. Relative elongation of the $[2](BF_4)_2$/CT-DNA system as a function of the C_D/C_P ratio. $C_P^0 = 2.00 \times 10^{-4}$ M, $C_D/C_P = 0 - 3.9$, $I = 2.5$ mM, pH = 6.0 and $T = 25$ °C.

The initial linear stretch, in which the relative viscosity increased with the C_D/C_P ratio, is associated with intercalation of the 2-pydaT ligand into DNA. The L/L_0 vs C_D/C_P plot (Figure 10) shows two linear intervals. According to Leszczynski et al.,[37] the intersection of the two branches corresponds to a critical C_D/C_P ratio, $r_{s,i}$, related to the extent of DNA unwinding, Φ_i, induced by the binding process[38] according to

dx.doi.org/10.1021/ic401197a | Inorg. Chem. 2013, 52, 9962−9974

Table 4. IC_{50} (μM) Values for Complex $[2](BF_4)_2$ and Reference Complexes Cisplatin, RM175 and RAPTA-C, in Cell Lines A2780, A2780cis, MCF-7, and MRC-5[a]

compound	pH_e	A2780	A2780cis	RF[b]	MCF-7	MRC-5	SF[c] (A2780)	SF[c] (A2780cis)
cisplatin	7.4	0.54 ± 0.01	7.09 ± 0.09	13.13 ± 0.03	10 ± 1	4.74 ± 0.11	8.78 ± 0.03	0.67 ± 0.01
RM175[d]		6[e]			93[e]			
RAPTA-C[e]		353 ± 12	252					
$[1](BF_4)$	7.4	8.60 ± 0.20						
$[2](BF_4)_2$	7.4	11 ± 1	3.05 ± 0.08	0.28 ± 0.01	134 ± 23	24 ± 1	2.18 ± 0.01	7.87 ± 0.07
$[2](BF_4)_2$	6.5	6.58 ± 0.48	1.45 ± 0.07	0.22 ± 0.01	96 ± 13			

[a]The values are given at two different pH values for $[2](BF_4)_2$. [b]RF = ratio of IC_{50} for A2780cis/IC_{50} for A2780. [c]SF = ratio of IC_{50} for MRC-5/IC_{50} for either A2780 or A2780cis. [d]IC_{50} values for RM175 from bibliography with exposure times of 24 h at standard pH.[13,43] [e]IC_{50} values for RAPTA-C from bibliography with exposure times of 96 h at standard pH.[44]

$$\Phi_i r_{s,i} = \text{cons} \quad (7)$$

For DNA/proflavine in water, the values of $\Phi_i\, r_{s,i} = 5.95$ with $\Phi = 17°$[32] and for ethidium bromide/DNA $\Phi = 26°$.[39] From Figure 10 it follows $r_s = 0.8$ and application of eq 7 yields the value $\Phi = 7.4°$ for $[2](BF_4)_2$/DNA. The limited ability of $[2](BF_4)_2$ to unwind DNA compared with the above systems confirms that in PD_{II}' intercalation of the 2-pydaT ligand into CT-DNA occurs only partially, consistent with the characteristics of the bifunctional complex (covalent-partly intercalated) put forward.

Thermal Denaturation Assays. As observed in Figure 15SI, Supporting Information, $[2](BF_4)_2$ stabilizes the DNA double helix. An asymptotic increase in the melting temperature from 69 to 75.7 °C was recorded when the C_D/C_P ratio was raised from zero to 1.0 (Figure 15SI, inset). Thermal stabilization is also characteristic of intercalating agents.[40]

The sets of data gathered, CD, viscometry, and thermal denaturation, unequivocally corroborate the kinetic assumptions, that is, formation of a stable intercalated-covalent bifunctional complex upon reaction of $[2](BF_4)_2$ with CT-DNA under the above-mentioned conditions.

Cytotoxicity. Liu and Sadler[41] have reported recently that the insertion of a coordinated aromatic ligand able to intercalate into DNA provides some metal complexes with a dual mode of binding, that is, intercalation between the DNA bases and metal coordination to a DNA base. This dual function induces unusual DNA distortions that affect the biological activity. The DNA structural changes can affect the recognition by repair enzymes and hence the downstream processes leading to apoptosis and cell death. Ru-arene complexes with such a dual mode of binding exhibit stronger cytotoxicity toward cancer cells than the nonintercalating counterparts.[41,42] On the other hand, Ru(II) aqua-complexes have not yet been tested as anticancer drugs, presumably because their high reactivity could prevent them from reaching the cells.

Bearing all this in mind, the cytotoxic activity of the aqua-complex $[2](BF_4)_2$ was studied in a comparative in vitro MTT cell viability assay with human ovarian carcinoma cells (A2780) and human breast adenocarcinoma cells (MCF-7). The study was performed by testing the drug at two different pH values of the growth medium, pH = 7.4 (standard for this cells) and pH = 6.5, in order to evaluate a possible pH effect on the citotoxicity as well. The activity values are expressed as the inhibitory potency (IC_{50}), which is the concentration of complex $[2](BF_4)_2$ required to decrease by 50% the cell viability (see Table 4).

The $[2](BF_4)_2$ complex displayed cytotoxic activity in the low micromolar range in the A2780 cell line, with an IC_{50} value only 20-fold higher than that for cisplatin (11 μM vs 0.54 μM), comparable to that of $[(\eta^6\text{-bip})Ru(en)(Cl)](PF_6)$ (referred as RM175 with bip = biphenyl; en = 1,2-diaminoethano), (11 μM vs 6 μM),[13,43] and much lower than those of $[(\eta^6\text{-}p\text{-cym})Ru(pta)(Cl_2)]$ (referred as RAPTA-C with pta = 1,3,5-triaza-7-phosphaadamantane), (11 μM vs 353 μM).[44] However, the activity in the MCF-7 cell line is very low. Anyhow, the inhibitory potency is pH-dependent, with IC_{50} values between 1.4-fold and 2-fold lower when the pH is decreased one unit (see Table 4) in A2780 and MCF-7. By contrast, no pH effect was observed on cell growth in similar studies with MCF-7 cells in the absence of drugs.[45]

The interesting pH-dependent antiproliferative activity of $[2](BF_4)_2$ can be related to its ability to interact with DNA at pH values below or close to its pK_{a1}, whereas the formation of the unreactive hydroxo derivative $[3]^+$ would account for the lower activity of the system at higher pH values.[18,19,46]

The cytotoxic activity of $[2](BF_4)_2$ was also tested in cisplatin-resistant human ovarian carcinoma cells (A2780cis) at normal (7.4) and acidic (6.5) pH. Remarkably, $[2](BF_4)_2$ is more active than cisplatin in this cell line, with an IC_{50} value 2-fold lower than that of the control drug, i.e., cisplatin (IC_{50} = 3.05 μM and IC_{50} = 7.09 μM respectively). The cell resistance factors (RF = ratio of IC_{50} for A2780cis/IC_{50} for A2780) is much better (lower) for $[2](BF_4)_2$ than for cisplatin (0.28 vs 13.13 respectively), meaning than this complex is not cross-resistant with cisplatin like other analogues recently reported by Sadler et al.[47] Once again, the activity was twice higher at acidic pH (Table 4).

Moreover, $[2](BF_4)_2$ displays a certain degree of selectivity for cancer cells (A2780 and A2780cis), versus normal human lung fibroblast cells (MRC-5). Indeed, the IC_{50} values for A2780 (11 μM) and A2780cis (3.05 μM) are lower than that for MRC-5 (24 μM). Thus, the complex is less toxic for healthy cells than cisplatin (4.74 μM). The cell selectivity factors for the aqua-complex (SF = ratio of IC_{50} for MRC-5/IC_{50} for either A2780 or A2780cis) are 2.18 in A2780 (worse than that for cisplatin, SF = 8.78) and 7.87 in A2780cis (better than that for cisplatin, SF = 0.67).

Rationalization of the biological results is by no means straightforward. Charged species have low rates of passive permeation through cell membranes.[48] However, different studies have shown that Ru(II) dicationic complexes can be rapidly transported across the cell membrane into the cytoplasma by passive diffusion, provided that they have either lipophilic groups (such as estradiol),[49] or cell-penetrating peptides (such as polyarginine chains)[50] attached to the ligands

dx.doi.org/10.1021/ic401197a | Inorg. Chem. 2013, 52, 9962−9974

Scheme 3. Intracellular Equilibria between $[1]^+$, $[2]^{2+}$, $[3]^+$, and the Ru-(DNA) Complexes PD_I and PD_{II}'

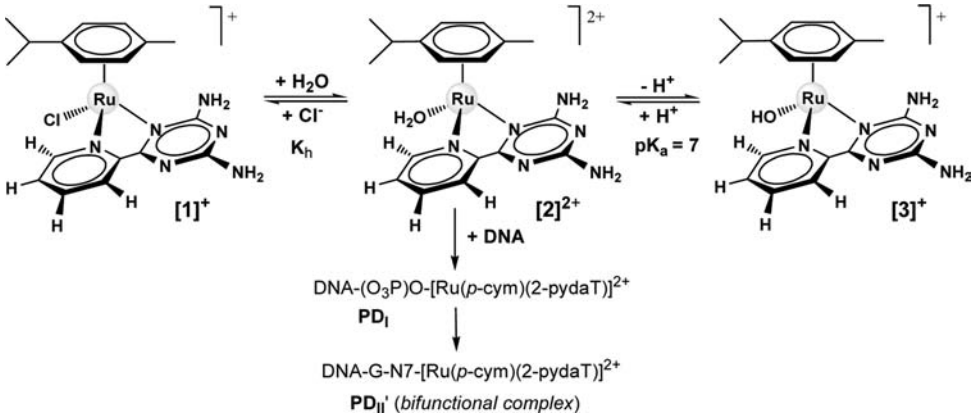

or as long as they bear heteropolyaromatic rings as ligands.[51] A similar uptake mechanism seems viable for $[\mathbf{2}](\mathbf{BF_4})_2$, considering the lipophilicity of the *p*-cymene ring. In the second place, dysregulated pH has been recognized as an adaptive feature of most cancers, meaning that in normal differentiated adult cells, intracellular pH (pH_i) is generally ~7.2 and lower than the extracellular pH (pH_e) of ~7.4, whereas cancer cells have higher pH_i (≥7.2) and lower pH_e (~6.7−7.1).[48,52,53] This "reversed" pH_i/pH_e gradient along with the chloride concentration, $[Cl^-]$, are thought to affect the drug distribution. In our case, the chlorido-species $[\mathbf{1}]^+$ and the dicationic aqua-derivative $[\mathbf{2}]^{2+}$ would be dominant in the acidic extracellular tumor space, with less abundance of the hydroxido-complex $[\mathbf{3}]^+$. On the contrary, in the cytoplasmic space and cell nucleus of cancer cells, where pH is higher and $[Cl^-]$ is lower, the concentration of the inert $[\mathbf{3}]^+$ form would be higher. Consequently, although this distribution profile could be detrimental to the interaction with the putative pharmacological target (DNA) and the corresponding cytotoxic drug action, we postulate that the equilibrium concentration of the active aqua-complex at pH~7.4 is high enough to allow the above dual interaction with DNA which would accordingly shift the equilibrium to left (Scheme 3). A similar behavior has been shown for $[(\eta^6\text{-}p\text{-arene})\mathrm{Ru(N{-}N)(L)}]^{n+}$ (L = Cl, H_2O, OH; en = ethylenediamine) complexes[18,19,54] and could be assumed for similar metallo-drugs, provided that the corresponding pK_a values of the aqua-derivatives are not very low.

CONCLUSIONS

A direct procedure to prepare the new aqua-complex $[(\eta^6\text{-}p\text{-cymene})\mathrm{Ru(OH_2)}(\kappa^2\text{-}N,N\text{-2-pydaT})](\mathrm{BF_4})_2$ $[\mathbf{2}](\mathbf{BF_4})_2$ is presented. The corresponding derivative with 9-methylguanine $[(\eta^6\text{-}p\text{-cymene})\mathrm{Ru}(\kappa^2\text{-}N,N\text{-2-pydaT})(N7\text{-9-MeG})](\mathrm{PF_6})_2$, $[\mathbf{4}](\mathbf{PF_6})_2$, has been isolated and its structure has been determined by X-ray diffraction. Concerning the interaction of $[\mathbf{2}](\mathbf{BF_4})_2$ with nucleotides, ^{1}H NMR, ^{31}P{^{1}H} NMR, and UV−vis kinetic experiments have shown that this species reacts with 2′-deoxyguanosine 5′-monophosphate (**5′-dGMP**) by a two-step mechanism; the first step, very fast, corresponds to the interaction between the Ru(II) center and the O-phosphate, whereas the second, slower step is attributed to a covalent interaction between the metal atom and the N7 guanine site of **5′-dGMP**. By contrast, the substitution processes over $[\mathbf{1}](\mathbf{BF_4})$ in the presence of free Cl^- are more arduous. Thus, aquation is a previous step to afford the guanine N7 adducts from $[\mathbf{1}](\mathbf{BF_4})$. The sets of experimental data gathered here (kinetic, CD, viscometry, and thermal denaturation) unequivocally corroborate the formation of a stable partially intercalated and covalent bifunctional complex with DNA, which involves the bonding of the $[(\eta^6\text{-}p\text{-cymene})\mathrm{Ru}(\kappa^2\text{-}N,N\text{-2-pydaT})]^{2+}$ fragment to the guanine residues of the CT-DNA. The formation of the Ru−O(PO_3) intermediate is the first step of the mechanism, the intercalated complex is formed in a second step and the stable covalent binding Ru−N7-G in a third, much slower step, yielding the bifunctional complex. A notable difference between $[\mathbf{1}](\mathbf{BF_4})$ and $[\mathbf{2}](\mathbf{BF_4})_2$ is that the former does not intercalate into CT-DNA despite the fact that 2-pydaT is also present in the chlorido-complex. The aqua-complex $[\mathbf{2}](\mathbf{BF_4})_2$ displays interesting and pH-dependent cytotoxic activity in human ovarian carcinoma cells (A2780) and to a lesser degree in human breast adenocarcinoma cells (MCF-7). Moreover, this derivative is 2-fold more active than cisplatin in cisplatin-resistant human ovarian carcinoma cells (A2780cis), showing a RF lower than 1 (RF = 0.28) and an increase in the activity with decreasing pH. A moderate selectivity toward the cancer cell lines A2780 and A2780cis over the model healthy human lung fibroblast cells (MRC-5) has been observed.

EXPERIMENTAL SECTION

Materials. Starting materials: $[(\eta^6\text{-}p\text{-cymene})\mathrm{Ru}(\mu\text{-Cl})\mathrm{Cl}]_2$,[55,56] $[(\eta^6\text{-}p\text{-cymene})\mathrm{RuCl}(\kappa^2\text{-}N,N\text{-2-pydaT})](\mathrm{BF_4})$, $[\mathbf{1}](\mathbf{BF_4})$,[16] and 2-pydaT[57] were prepared according to the literature. $AgBF_4$, 9-methylguanine, 2′-deoxyguanosine 5′-monophosphate (**5′-dGMP**), 2′-deoxyadenosine 5′-monophosphate (**5′-dAMP**), and Calf thymus DNA (CT-DNA) were purchased from Aldrich and used without further purification. Deuterated solvents were obtained from SDS and Euriso-top. Solutions of $[(\eta^6\text{-}p\text{-cymene})\mathrm{Ru(OH_2)}(\kappa^2\text{-}N,N\text{-2-pydaT})](\mathrm{BF_4})_2$, $[\mathbf{2}](\mathbf{BF_4})_2$, were always freshly prepared by dissolving weighed amounts of the solid into the buffer solution, the resulting concentration referred to as C_D. Solutions of doubly deionized water (Millipore Q, APS; Los Angeles, California) containing 2.5 mM sodium cacodylate ($Na(CH_3)_2AsO_2$) were used as a buffer to maintain the pH constant at 6.0. The CT-DNA lyophilized sodium salt was dissolved into doubly deionized water and sonicated with an MSE-Sonyprep sonicator, by applying to suitable CT-DNA samples (10 mL of CT-DNA 2.3×10^{-3} M) 20 repeated cycles of 10 s sonication and 20 s pause at an amplitude of 98 μm. The sonicator tip was introduced directly into a solution kept in an ice bath to minimize sonication thermal effects. Agarose gel electrophoresis tests indicate that the DNA length was reduced to roughly 1000 base-pairs. The CT-DNA stock solutions were standardized spectrophotometrically using ε = 13 200 $M^{-1}\,cm^{-1}$ (260 nm).[58] The polynucleotide concentration is expressed in molarity of base pairs (M_{BP}) and denoted as C_P.

dx.doi.org/10.1021/ic401197a | Inorg. Chem. 2013, 52, 9962−9974

Methods. All synthetic manipulations were carried out under dry oxygen-free nitrogen atmosphere using standard Schlenk techniques. The solvents were distilled from the appropriate drying agents and degassed before use. Elemental analyses were performed with a Perkin-Elmer 2400 CHN microanalyzer. The analytical data for the new aqua-complex was obtained from a crystalline sample, showing sufficient analytical purity to be used as the starting material. IR spectra were recorded on a Nicolet Impact 410 spectrophotometer (4000−400 cm^{-1}) as KBr pellets and on a Jasco FT/IR-6300 spectrophotometer (650−160 cm^{-1} range) as Nujol mulls deposited on polyethylene films. Fast atom bombardment mass spectra (FAB MS) were recorded with an Autospec spectrometer (peaks position in DA). NMR samples were prepared in a nitrogen atmosphere by dissolving suitable amounts of the corresponding compounds in 0.5 mL of the respective oxygen-free deuterated solvent, and the spectra were recorded at 298 K (unless otherwise stated) on a Varian Unity Inova-400 (400 MHz for ^{1}H; 376 MHz for ^{19}F; 161.9 MHz for ^{31}P; 100.6 MHz for ^{13}C). Typically, 1D ^{1}H NMR spectra were acquired with 32 scans into 32 k data points over a spectral width of 16 ppm. ^{1}H and $^{13}C\{^{1}H\}$ NMR chemical shifts were internally referenced to TMS via 1,4-dioxane in D_2O (δ = 3.75 ppm and δ = 67.19 ppm, respectively) according to the values reported by Fulmer et al.[59] All ^{31}P resonances were referenced to 85% H_3PO_4 at 0 ppm. Chemical shift values are reported in ppm and coupling constants (J) in Hertz. The proton resonance splitting in the ^{1}H NMR data is defined as s = singlet, d = doublet, t = triplet, q = quartet, sept = septet, m = multiplet, bs = broad singlet. 2D spectra were recorded using standard pulse−pulse sequences. COSY spectra: standard pulse sequence, acquisition time 0.214 s, pulse width 10 μs, relaxation delay 1 s, 16 scans, 512 increments. The NOESY spectra were recorded with 5000 Hz, acquisition time 3.27 s, 90° pulse width, 4 s relaxation delay, and 5−10 dB irradiation power. The probe temperature (±1 K) was controlled by a standard unit calibrated with a methanol reference. Processing of all NMR data was carried out using MestReNova version 6.1.1.

X-ray Crystallography. A summary of crystal data collection and refinement parameters for all compounds are given in Table 4SI, Supporting Information. Single crystals of $[\mathbf{1}](\mathbf{PF_6})$ and $[\mathbf{4}](\mathbf{PF_6})_2$ were mounted on a glass fiber and transferred to a Bruker X8 APEX II CCD-based diffractometer equipped with a graphite monochromated Mo Kα radiation source (λ = 0.71073 Å). The highly redundant data sets were integrated using SAINT[60] and corrected for Lorentz and polarization effects. The absorption correction was based on the function fitting to the empirical transmission surface as sampled by multiple equivalent measurements with the program SADABS.[61]

The software package SHELXTL version 6.10[62] was used for space group determination, structure solution, and refinement by full-matrix least-squares methods based on F^2. A successful solution by direct methods provided most non-hydrogen atoms from the E-map. The remaining non-hydrogen atoms were located in an alternating series of least-squares cycles and difference Fourier maps. All non-hydrogen atoms were refined with anisotropic displacement coefficients. Hydrogen atoms were placed using a "riding model" and included in the refinement at calculated positions. CCDC reference numbers for $[\mathbf{1}](\mathbf{PF_6})$ (913600) and for $[\mathbf{4}](\mathbf{PF_6})_2$ (938281).

pH Measurements. These were performed at 25 °C with a Metrohm 16 DMS Titrino pH-meter fitted with a combined glass electrode with 3 M KCl as liquid junction. The pH was adjusted with NaOH or $HClO_4$. The pH values of NMR samples in D_2O were obtained before and after recording the NMR spectra. No correction has been applied for the effect of deuterium on the glass electrode.

Conductivity Measurements. The Λ_M values are given in $S{\cdot}cm^2{\cdot}mol^{-1}$ and were obtained at room temperature for 10^{-3} M solutions of the corresponding complexes in CH_3CN, using a CRISON conductometer 522 equipped with a CRISON platinum conductivity cell 5292.

Aqueous Solution Chemistry. The aquation-anation equilibrium of the Ru^{II} chloride complex $[\mathbf{1}](\mathbf{BF_4})$ was monitored by ^{1}H NMR spectroscopy. The spectra were recorded for 18 mM solutions in D_2O at various time intervals, and the signals were referenced to TMS via 1,4-dioxane as an internal reference (δ = 3.75 ppm). The relative amounts of the Ru^{II} chloride complex and the aquo derivative were determined by integration of the respective ^{1}H resonances.

Thermal Denaturation and Spectrophotometric Measurements. These were performed using a Hewlett-Packard 8453A spectrophotometer (Agilent Technologies, Palo Alto, CA, USA) fitted with a photodiode array detection and Peltier temperature control systems. The pK_a values were evaluated analyzing the absorbance change of a 9.0×10^{-5} M $[\mathbf{2}](\mathbf{BF_4})_2$ solution recorded at different pH values. The melting experiments were carried out using a 3.1×10^{-5} M CT-DNA solution varying the C_D/C_P ratio from 0 to 1, recording the absorbance spectra while heating from 40 to 95 °C at 0.3 °C/min.

Circular Dichroism Titrations. The CD spectra were recorded using a MOS-450 Bio-Logic spectrophotometer (Claix, France). The measurements were performed in 1.0 cm path-length cells at 25 °C. Titrations were carried out adding microamounts of $[\mathbf{2}](\mathbf{BF_4})_2$ to a CT-DNA solution 1.0×10^{-4} M waiting 2 h per addition.

Viscosity Measurements. These were performed using a Micro-Ubbelohde viscometer whose temperature was controlled by an external thermostat (25 ± 0.1 °C). The viscosity data were analyzed by the expression $L/L_0 = (\eta/\eta_0)^{1/3}$. Relative viscosities were measured using $\eta/\eta_0 = (t - t_0)/(t_{DNA} - t_0)$, where t_0 and t_{DNA} are the flow time of the solvent and DNA solution, respectively, and t is the flow time of the $[\mathbf{2}](\mathbf{BF_4})_2$ and DNA mixture after 2 h stabilization period. Mean values of replicated measurements were used to evaluate the sample viscosity, η, and that of DNA alone, η_0.[36]

Stopped Flow Experiments. These were performed at 25 °C, I = 2.5 mM and pH = 6.0 in a stopped flow Bio-Logic SFM-300 spectrophotometer with absorbance detection system and dead time below 3 ms. The kinetic curves, obtained averaging out at least five shots, were analyzed with the Jandel (AISN software, Mapleton, OR) fitting package.

Cell Culture. Frozen MCF-7 cells were thawed out in a 75 cm^2 cell culture flask in EMEM supplemented with 2-mM L-glutamine, 1.5 g/L $NaHCO_3$, 0.1 mM nonessential aminoacids, 1 mM sodium pyruvate, 0.01 mg/mL bovine insuline, and 10% FBS and maintained at 37 °C in 5% CO_2 atmosphere, replacing the medium twice a week. Frozen MRC-5 cells were thawed in a 75 cm^2 cell culture flask in EMEM supplemented with 10% FBS and maintained at 37 °C in a 5% CO_2 atmosphere, replacing medium twice a week. Frozen A2780cis cells were thawed in a 75 cm^2 cell culture flask in RPMI 1640 medium supplemented with 2 mM L-glutamine and 10% FBS and maintained at 37 °C in a 5% CO_2 atmosphere, replacing the medium twice a week.

Cytotoxicity Assays. The MTT proliferation assay is based on the reduction of the yellow MTT tetrazolium salt (3-[4,5-dimethylthiazol-2-yl]-2,5diphenyltetrazolium bromide) by mitochondrial dehydrogenases to form a blue MTT formazan in viable cells.[63] Approximately 4×10^3 cells per well for either A2780 and A2780cis and 1×10^4 cells per well for either MCF-7 and MRC-5 were cultured in 100 μL of growth medium in 96-well plates and incubated at 37 °C under 5% CO_2 atmosphere. The cells were grown for 24 h, and the growth medium was replaced by fresh medium containing different concentrations of the compounds to be assayed and maintained at 37 °C in a 5% CO_2 atmosphere for either 96 h (MCF-7 or A2780cis cell lines) or 168 h (MRC-5 cell line). Cisplatin was used as a positive control. After this time, 10 μL of a 5 mg/mL of MTT in PBS (0.136 mM NaCl, 1.47 mM KH_2PO_4, 8 mM NaH_2PO_4, 2.68 mM KCl) was added to each well, and the cells were maintained at 37 °C in 5% CO_2 atmosphere for 4 h. Afterward, 100 μL of a 10% SDS solution in 0.01 M HCl was added to each well, and the cells were maintained at 37 °C in a 5% CO_2 atmosphere for 12−14 h. Absorbance was read at λ = 595 nm in an Ultra-Evolution microplate reader (Tecan). At least two independent experiments were performed with three replicates per dose. The data were expressed as the growth inhibition percentage calculated according to the equation: % growth inhibition = $100 - ((A_D \times 100)/A_B)$, where A_D is the measured absorbance in wells containing samples and A_B is the absorbance measured for blank wells (cells with medium and vehicle). To calculate the growth inhibitory potency of the compounds, concentration−response curves of the compounds were constructed and fitted to the following equation:

dx.doi.org/10.1021/ic401197a | Inorg. Chem. 2013, 52, 9962−9974

$$y = \frac{E_{max}}{1 + \left(\frac{IC_{50}}{x}\right)^n}$$

where y is the % growth inhibitory effect, E_{max} is the maximal inhibitory effect observed, IC_{50} is the concentration of the compound inhibiting the growth in a 50%, n is the slope of the fitting, and x is the drug concentration. Nonlinear regression was carried out by GraphPad Prism, version 2.01, 1996 (GraphPad Software Inc.).

Synthesis of [(η^6-p-cymene)Ru(OH_2)(κ^2-N,N-2-pydaT)](BF_4)$_2$, [2](BF_4)$_2$. $AgBF_4$ in excess (48.2 mg, 0.25 mmol) was added to a suspension of [**1**](**BF_4**) (100 mg, 0.18 mmol) in water (10 mL), and the mixture was stirred and heated at 50 °C for 20 h, using a darkened Schlenk flask. Stirring was stopped and the mixture was cooled to room temperature. The AgCl content was filtered and the solvent was evaporated to dryness under vacuum. The residue was washed with diethylether (10 mL), and the resulting yellow solid was dried under vacuum. Yield: 55.2 mg (0.09 mmol, 49%). M_r ($C_{18}H_{24}N_6ORuB_2F_8$): 615.1044 g·mol^{-1}. Anal. Calcd. for $C_{18}H_{24}N_6ORuB_2F_8 \cdot 2.25H_2O$: C, 32.98; H, 4.38; N, 12.82; Found: C, 32.81; H, 4.32; N, 13.17 (see Scheme 1 for numbering). ^{1}H NMR (400 MHz, D_2O, pH = 3.9, 25 °C) δ = 9.54 (m, H$^{6'}$-py, 1H), 8.48 (m, H$^{3'}$-py, 1H), 8.32 (m, H$^{4'}$-py, 1H), 7.97 (m, H$^{5'}$-py, 1H), 6.40 (d, ^3J = 6.2 Hz, H^2-cym, 1H), 6.14 (m, H^{5,6}-cym, 2H), 6.01 (d, ^3J = 6.2 Hz, H^3-cym, 1H), 2.49 (sept, ^3J = 6.9 Hz, H^7-cym, 1H), 2.26 (s, H^{10}-cym, 3H), 1.04 (d, ^3J = 6.8 Hz, H^8-cym, 3H), 0.93 (d, ^3J = 6.9 Hz, H^9-cym, 3H) ppm. ^{13}C{^{1}H} NMR (101 MHz, D_2O, pH = 3.9, 25 °C) δ = 170.42 (s, C^{t6}-tz, 1C), 166.24 (s, C^{t2}-tz, 1C), 166.06 (s, C^{t4}-tz, 1C), 156.26 (s, C$^{6'}$-py, 1C), 153.65 (s, C$^{2'}$-py, 1C), 142.20 (s, C$^{4'}$-py, 1C), 131.52 (s, C$^{5'}$-py, 1C), 127.57 (s, C$^{3'}$-py, 1C), 105.96 (s, C^4-cym, 1C), 100.26 (s, C^1-cym, 1C), 87.46 (s, C^{6,2}-cym, 2C), 83.29 (s, C^5-cym, 1C), 81.76 (s, C^3-cym, 1C), 31.02 (s, C^7-cym, 1C), 21.93 (s, C^8-cym, 1C), 21.51 (s, C^9-cym, 1C), 18.22 (s, C^{10}-cym, 1C) ppm. ^{19}F NMR (376 MHz, D_2O, pH = 3.9, 25 °C) δ = −154.83 (s, ^{10}B−F), −154.88 (s, ^{11}B−F) ppm. FT-IR (KBr, cm^{-1}): 3457, 3365, 2972, 2928, 1631, 1588, 1566, 1520, 1400, 1083, 787, 759 523. FT-IR (nujol, cm^{-1}): 302, 254, 247, 242, 208, 201, 194, 187, 177, 166. Molar conductivity (CH_3CN): 284 S·cm^2·mol^{-1}. Solubility: soluble in methanol, ethanol and water. Mass FAB+ (MeOH): m/z (%) = 443 (100) ([M + H-2BF_4]$^+$ = [$C_{18}H_{25}ON_6Ru$]$^+$); 423 (48) ([M − OH_2-H-2BF_4]$^+$ = [$C_{18}H_{21}N_6Ru$]$^+$).

Synthesis of [(η^6-p-cymene)Ru(N7-9-MeG)(κ-N,N-2-pydaT)](PF_6)$_2$, [4](PF_6)$_2$. In a 100 mL Schlenk flask a suspension of [**1**](**BF_4**) (32.7 mg, 0.06 mmol) in degassed water (10 mL) was stirred for 2 h at room temperature under nitrogen atmosphere. Then, **9-MeG** (11.4 mg, 0.07 mmol) was added, and the mixture was stirred at 37 °C for 16 h to produce a yellow solution, which was filtered to remove solid impurities. NH_4PF_6 (27.4 mg, 0.17 mmol) was then added to the resulting solution, and the mixture was stirred for 1 h. Solid impurities were removed by filtration, and the solution was concentrated under a vacuum to precipitate a yellow-orange product that was filtered, washed with diethylether, and dried under a vacuum to give a yellow solid. Yield: 29.3 mg (0.03 mmol, 56%). M_r ($C_{24}H_{29}N_{11}ORuP_2F_{12}$): 878.5645 g·mol^{-1}. ^{1}H NMR (400 MHz, D_2O, 25 °C) δ = 9.67 (m, H$^{6'}$-py, 1H), 8.50 (m, H$^{3'}$-py, 1H), 8.32 (m, H$^{4'}$-py, 1H), 8.00 (m, H$^{5'}$-py, 1H), 6.81 (s, H$^{8''}$-9-MeG, 1H), 6.45 (d, ^3J = 6.2 Hz, H^2-cym, 1H), 6.21 (m, H^{5,6}-cym, 2H), 5.98 (d, ^3J = 6.2 Hz, H^3-cym, 1H), 3.45 (s, N-Me, 3H), 2.58 (sept, ^3J = 6.9 Hz, H^7-cym, 1H), 2.00 (s, H^{10}-cym, 3H), 1.05 (d, ^3J = 6.8 Hz, H^8-cym, 3H), 0.88 (d, ^3J = 6.9 Hz, H^9-cym, 3H) ppm. ^{19}F NMR (376 MHz, D_2O, 25 °C) δ = −72.53 (d, $^1J_{PF}$ = 710 Hz, PF_6^-) ppm. The ^{1}H NMR spectrum of the crude showed traces of [**1**]$^+$ and [**2**]$^{2+}$, and crystallization experiments afforded a single crystal of [**1**](**PF_6**).

NMR Reactivity Experiments. Typical reactivity NMR experiments were performed as follows. Reaction of [**2**](**BF_4**)$_2$ with **9-MeG**. The solutions of both reactants were prepared independently, and the pH was adjusted to 7.0 prior to mixing. Solution A: [**2**](**BF_4**)$_2$ (20 mM) was dissolved in D_2O (0.25 mL with 1,4-dioxane, 5%) in an Eppendorf, and the pH was set to 7.0 by addition of NaOH (0.1 and 0.01 M). Solution B: 9-MeG (40 mM) was dissolved in D_2O (0.25 mL with 1,4-dioxane, 5%) in an Eppendorf, and the pH was set to 7 by addition of $HClO_4$ (0.1 M) and NaOH (0.1 and 0.01 M). Solutions A and B were mixed and transferred to an NMR tube. A ^{1}H NMR spectrum was immediately recorded, and then the reaction was monitored. ^{1}H NMR data in D_2O for the resulting [(η^6-p-cymene)Ru(N7-9-MeG)(κ^2-N,N-2-pydaT)](BF_4)$_2$, [**4**](**BF_4**)$_2$, are coincident with those of isolated [**4**](**PF_6**)$_2$.

■ ASSOCIATED CONTENT

Ⓢ Supporting Information

NMR spectra for additional reactivity experiments with nucleobases and nucleotides, H-bonding data and crystallographic parameters for [**1**](**PF_6**), graphics for additional kinetic experiments, melting profiles and T_m values. This material is available free of charge via the Internet at http://pubs.acs.org.

■ AUTHOR INFORMATION

Corresponding Author

*(G.E.) Fax: (+) 947-258831. E-mail: gespino@ubu.es. (B.G.) E-mail: begar@ubu.es. Fax: (+) 947-258831.

Notes

The authors declare no competing financial interest.

■ ACKNOWLEDGMENTS

The financial support by the Spanish MICINN (CTQ2011-24434 and CTQ2009-13051/BQU, partially supported by FEDER), the Junta de Castilla y León (Fondo Social Europeo, project BU-299A12-1), and Obra Social "la Caixa" are gratefully acknowledged. Thanks are due to J. Delgado, P. Castroviejo, and M. Mansilla from PCI of Burgos University for technical support. G.E. also wants to acknowledge M. Pérez-Manrique for her inspiring example.

■ REFERENCES

(1) Rosenberg, B.; van Camp, L.; Trosko, J. E.; Mansour, V. H. *Nature* **1969**, *222*, 385−386.
(2) Ahmad, S. *Chem. Biodiversity* **2010**, *7*, 543−566.
(3) Kelland, L. *Nat. Rev. Cancer* **2007**, *7*, 573−584.
(4) Jamieson, E. R.; Lippard, S. J. *Chem. Rev.* **1999**, *99*, 2467−2498.
(5) Rosenberg, B. *Adv. Exp. Med. Biol.* **1977**, *91*, 129−50.
(6) Bruijnincx, P. C. A.; Sadler, P. J. *Curr. Opin. Chem. Biol.* **2008**, *12*, 197−206.
(7) Georgiades, S. N.; Vilar, R. *Annu. Rep. Prog. Chem., Sect. A: Inorg. Chem.* **2010**, *106*, 481−503.
(8) Suntharalingam, K.; Vilar, R. *Annu. Rep. Prog. Chem., Sect. A: Inorg. Chem.* **2011**, *107*, 339−358.
(9) Thompson, K. H.; Orvig, C. *Dalton Trans.* **2006**, 761−764.
(10) Bergamo, A.; Gaiddon, C.; Schellens, J. H. M.; Beijnen, J. H.; Sava, G. *J. Inorg. Biochem.* **2012**, *106*, 90−99.
(11) Antonarakis, E.; Emadi, A. *Cancer Chemother. Pharmacol.* **2010**, *66*, 1−9.
(12) Bergamo, A.; Sava, G. *Dalton Trans.* **2007**, 1267−1272.
(13) Bergamo, A.; Masi, A.; Peacock, A. F. A.; Habtemariam, A.; Sadler, P. J.; Sava, G. *J. Inorg. Biochem.* **2010**, *104*, 79−86.
(14) Ang, W.-H.; Casini, A.; Sava, G.; Dyson, P. J. *J. Organomet. Chem.* **2011**, *696*, 989−998.
(15) Aliende, C.; Pérez-Manrique, M.; Jalón, F. A.; Manzano, B. R.; Rodriguez, A. M.; Cuevas, J. V.; Espino, G.; Martinez, M. A.; Massaguer, A.; Gonzalez-Bartulos, M.; de Llorens, R.; Moreno, V. *J. Inorg. Biochem.* **2012**, *117*, 171−188.
(16) Busto, N.; Valladolid, J.; Aliende, C.; Jalon, F. A.; Manzano, B. R.; Rodriguez, A. M.; Gaspar, J. F.; Martins, C.; Biver, T.; Espino, G.; Leal, J. M.; García, B. *Chem.-Asian J.* **2012**, *7*, 788−801.
(17) Novakova, O.; Chen, H.; Vrana, O.; Rodger, A.; Sadler, P. J.; Brabec, V. *Biochemistry* **2003**, *42*, 11544−11554.
(18) Wang, F.; Chen, H.; Parsons, S.; Oswald, I. D. H.; Davidson, J. E.; Sadler, P. J. *Chem.—Eur. J.* **2003**, *9*, 5810−5820.

(19) Chen, H.; Parkinson, J. A.; Morris, R. E.; Sadler, P. J. *J. Am. Chem. Soc.* **2003**, *125*, 173−186.
(20) García, B.; Ibeas, S.; Muñoz, A.; Leal, J. M.; Ghinami, C.; Secco, F.; Venturini, M. *Inorg. Chem.* **2003**, *42*, 5434−5441. Geary, W. J. *Coord. Chem. Rev.* **1971**, *7*, 81−122.
(21) Domingo, P. L.; Garcia, B.; Leal, J. M. *Can. J. Chem.* **1987**, *65*, 583−589. García, B.; Ibeas, S.; Leal, J. M. *J. Phys. Org. Chem.* **1996**, *9*, 593−597.
(22) Peacock, A. F. A.; Habtemariam, A.; Moggach, S. A.; Prescimone, A.; Parsons, S.; Sadler, P. J. *Inorg. Chem.* **2007**, *46*, 4049−4059.
(23) Betanzos-Lara, S.; Novakova, O.; Deeth, R.; Pizarro, A.; Clarkson, G.; Liskova, B.; Brabec, V.; Sadler, P.; Habtemariam, A. *J. Biol. Inorg. Chem.* **2012**, *17*, 1033−1051.
(24) Scheller, K. H.; Scheller-Krattiger, V.; Martin, R. B. *J. Am. Chem. Soc.* **1981**, *103*, 6833−6839.
(25) Peacock, A. F. A.; Habtemariam, A.; Fernández, R.; Walland, V.; Fabbiani, F. P. A.; Parsons, S.; Aird, R. E.; Jodrell, D. I.; Sadler, P. J. *J. Am. Chem. Soc.* **2006**, *128*, 1739−1748.
(26) Bugarcic, T.; Habtemariam, A.; Stepankova, J.; Heringova, P.; Kasparkova, J.; Deeth, R. J.; Johnstone, R. D. L.; Prescimone, A.; Parkin, A.; Parsons, S.; Brabec, V.; Sadler, P. J. *Inorg. Chem.* **2008**, *47*, 11470−11486.
(27) Hanif, M.; Henke, H.; Meier, S. M.; Martic, S.; Labib, M.; Kandioller, W.; Jakupec, M. A.; Arion, V. B.; Kraatz, H.-B.; Keppler, B. K.; Hartinger, C. G. *Inorg. Chem.* **2010**, *49*, 7953−7963.
(28) Zobi, F.; Hohl, M.; Zimmermann, I.; Alberto, R. *Inorg. Chem.* **2004**, *43*, 2771−2772.
(29) Burgess, J. *Metal Ions in Solution*; Ellis Horwood Ltd.: Chichester: New York, 1978; p 481.
(30) Diebler, H.; Secco, F.; Venturini, M. *Biophys. Chem.* **1987**, *26*, 193−205.
(31) Lepecq, J. B.; Paoletti, C. *J. Mol. Biol.* **1967**, *27*, 87−106.
(32) García, B.; Leal, J. M.; Ruiz, R.; Biver, T.; Secco, F.; Venturini, M. *J. Phys. Chem. B* **2010**, *114*, 8555−8564.
(33) Biver, T.; Secco, F.; Venturini, M. *Coord. Chem. Rev.* **2008**, *252*, 1163−1177.
(34) Zimmer, C.; Luck, G. Use of circular dichroism to probe DNA structure and drug binding to DNA. In *Advances in DNA Sequence-specific Agents*; Hurley, L. H., Ed. Elsevier: Amsterdam, 1992; Vol. *1*.
(35) Busto, N.; García, B.; Leal, J. M.; Secco, F.; Venturini, M. *Org. Biomol. Chem.* **2012**, *10*, 2594−2602.
(36) Cohen, G.; Eisenberg, H. *Biopolymers* **1969**, *8*, 45−55.
(37) Leszczynski, T.; Dunski, H. *Zesz. Nauk. - Politech. Lodz., Chem. Spozyw. Biotechnol.* **2006**, *70*, 13−22.
(38) Cantor, C. R.; Schimmel, P. R. *Biophysical Chemistry*.: W.H. Freeman: San Francisco, 1985.
(39) Graves, D. E.; Velea, L. M. *Curr. Org. Chem.* **2000**, *4*, 915−929.
(40) Busto, N.; García, B.; Leal, J. M.; Gaspar, J. F.; Martins, C.; Boggioni, A.; Secco, F. *Phys. Chem. Chem. Phys.* **2011**, *13*, 19534−19545.
(41) Liu, H.-K.; Sadler, P. J. *Acc. Chem. Res.* **2011**, *44*, 349−359.
(42) Bugarcic, T.; Novakova, O.; Halamikova, A.; Zerzankova, L.; Vrana, O.; Kasparkova, J.; Habtemariam, A.; Parsons, S.; Sadler, P. J.; Brabec, V. *J. Med. Chem.* **2008**, *51*, 5310−5319.
(43) Morris, R. E.; Aird, R. E.; Murdoch, P. D.; Chen, H. M.; Cummings, J.; Hughes, N. D.; Parsons, S.; Parkin, A.; Boyd, G.; Jodrell, D. I.; Sadler, P. J. *J. Med. Chem.* **2001**, *44* (22), 3616−3621.
(44) (a) Renfrew, A. K.; Phillips, A. D.; Egger, A. E.; Hartinger, C. G.; Bosquain, S. S.; Nazarov, A. A.; Keppler, B. K.; Gonsalvi, L.; Peruzzini, M.; Dyson, P. J. *Organometallics* **2009**, *28* (4), 1165−1172. (b) Renfrew, A. K.; Phillips, A. D.; Tapavicza, E.; Scopelliti, R.; Rothlisberger, U.; Dyson, P. J. *Organometallics* **2009**, *28* (17), 5061−5071. (c) Ang, W. H.; Grote, Z.; Scopelliti, R.; Juillerat-Jeanneret, L.; Severin, K.; Dyson, P. J. *J. Organomet. Chem.* **2009**, *694* (6), 968−972.
(45) Mahoney, B. P.; Raghunand, N.; Baggett, B.; Gillies, R. J. *Biochem. Pharmacol.* **2003**, *66*, 1207−1218.
(46) Pizarro, A. M.; Melchart, M.; Habtemariam, A.; Salassa, L.; Fabbiani, F. P. A.; Parsons, S.; Sadler, P. J. *Inorg. Chem.* **2010**, *49*, 3310−3319.
(47) Romero-Canelón, I.; Salassa, L.; Sadler, P. J. *J. Med. Chem.* **2013**, *56*, 1291−1300.
(48) Webb, B. A.; Chimenti, M.; Jacobson, M. P.; Barber, D. L. *Nat. Rev. Cancer* **2011**, *11*, 671−677.
(49) Lo, K. K.-W.; Lee, T. K.-M.; Lau, J. S.-Y.; Poon, W.-L.; Cheng, S.-H. *Inorg. Chem.* **2008**, *47*, 200−208.
(50) Neugebauer, U.; Pellegrin, Y.; Devocelle, M.; Forster, R. J.; Signac, W.; Moran, N.; Keyes, T. E. *Chem. Commun.* **2008**, 5307−5309.
(51) Puckett, C. A.; Barton, J. K. *Biochemistry* **2008**, *47*, 11711−11716.
(52) Gallagher, F. A.; Kettunen, M. I.; Day, S. E.; Hu, D.-E.; Ardenkjaer-Larsen, J. H.; Zandt, R. i. t.; Jensen, P. R.; Karlsson, M.; Golman, K.; Lerche, M. H.; Brindle, K. M. *Nature* **2008**, *453*, 940−943.
(53) Gillies, R. J.; Raghunand, N.; Karczmar, G. S.; Bhujwalla, Z. M. *J. Magn. Reson. Imaging* **2002**, *16*, 430−450.
(54) Ginzinger, W.; Mühlgassner, G.; Arion, V. B.; Jakupec, M. A.; Roller, A.; Galanski, M.; Reithofer, M.; Berger, W.; Keppler, B. K. *J. Med. Chem.* **2012**, *55*, 3398−3413.
(55) Zelonka, R. A.; Baird, M. C. *Can. J. Chem.* **1972**, *50*, 3063−3072.
(56) Bennett, M. A.; Smith, A. K. *J. Chem. Soc., Dalton Trans.* **1974**, 233−241.
(57) Case, F. H.; Koft, E. *J. Am. Chem. Soc.* **1959**, *81*, 905−906.
(58) Reichmann, M. E.; Rice, S. A.; Thomas, C. A.; Doty, P. *J. Am. Chem. Soc.* **1954**, *76*, 3047−3053.
(59) Fulmer, G. R.; Miller, A. J. M.; Sherden, N. H.; Gottlieb, H. E.; Nudelman, A.; Stoltz, B. M.; Bercaw, J. E.; Goldberg, K. I. *Organometallics* **2010**, *29*, 2176−2179.
(60) *SAINT Area-Detector Integration Program*, SAINT+ v7.12a.; Bruker AXS: Madison, Wisconsin, USA, 2004.
(61) Sheldrick, G. M. *SADABS A Program for Empirical Absorption Correction*, version 2004/1; University of Göttingen: Göttingen, Germany, 2004.
(62) *SHELXTL-NT Structure Determination Package*, version 6.12; Bruker AXS: Madison, Wisconsin, USA, 2001.
(63) Carmichael, J.; DeGraff, W. G.; Gazdar, A. F.; Minna, J. D.; Mitchell, J. B. *Cancer Res.* **1987**, *47*, 943−946.